Lithium and Cerium based sol-gel coatings for corrosion protection of AA2024-T3

DELFT UNIVERSITY OF TECHNOLOGY

MASTER THESIS REPORT

(MS53000)

Author: Shuai He (student number: 4815335)

Supervisor: Prof.dr.ir. JMC(Arjan) Mol
Daily Supervisor: Dr. Urša Tiringer

Faculty of Mechanical, Maritime and Materials Engineering

Department of Materials Science and Engineering

August 26, 2020

TUDelft Delft
University of
Technology

Abstract

Due to the demand of reducing the weight of aircrafts to reduce the carbon consumptions without compromising the mechanical properties, aluminium alloy AA2024-T3 has been widely applied in the aircrafts' manufacture. However, the alloying elements which ensure the mechanical properties also could increase the susceptibility of localized corrosion. The chromate conversion coatings (CCCs) have been used as the efficient anti-corrosion protection for aluminium alloys. Due to their toxicity, many countries and regions in the world have been banned CCCs from many industries. Numerous alternatives were studied for decades to replace the CCCs. Among all of them, the sol-gel technology is a promising method to inhibit the corrosion of aluminium alloy AA2024-T3. Furthermore, the addition of corrosion inhibitor into the sol-gel coating additionally increases active corrosion protection of aluminium alloys.

This thesis focuses on the sol-gel coatings corrosion protection of aluminium alloy AA2024-T3 with the incorporation of lithium and cerium salt as corrosion inhibitors.

The corrosion protection for the intact coatings was analyzed by potentiodynamic polarization measurements and electrochemical impedance spectroscopy (EIS). An active corrosion protection for the scribed coatings was investigated by observation of immersion test with digital optical microscope and the electrochemical impedance spectroscopy (EIS).

 The main findings of the present work are the following: (1) the sol-gel coating decreases the corrosion. (2) the addition of corrosion inhibitors, $LiNO_3$ and $Ce(NO_3)_3$, into the sol-gel coating decreases the corrosion current. (3) the combination of $LiNO_3$ and $Ce(NO_3)_3$ provides the best corrosion protection for intact coatings applied on AA2024-T3.

Contents

List of Figures

List of Tables

1 Introduction

Aluminium belongs to the group of lightweight metals and is widely used in transportation industry. Aluminium is the most abundant metal element and is the third common element, comprising about 8% of the crust [1]. Pure aluminium has good electrical and thermal conductivity and good corrosion resistant.[2]. However, alloying with other elements could produce other desired mechanical properties such as high strength for other applications [3]. In aluminum alloys selected alloying elements, e.g. copper, manganese, silicon, magnesium and zinc, are added to pure aluminum to obtain the desired properties for specific applications in industries [3]. Alloying elements represent so called intermetallic particles of alloys. Due to the presence of intermetallic particles, aluminium alloys are susceptible to corrosion, when exposed to specific environment condition [4]. Thus, the corrosion protection industry is required to investigate the corrosion protective scheme for corrosion protection of aluminium alloys to guarantee the stability and lifespan of aircrafts' structure [5]. For the last six decades, chromium conversion coatings (CCCs) have been the most efficient corrosion protection for aluminium alloys. However, their use is restricted in many industries because of their toxicity and carcinogenic properties [4]. One of the promising alternatives for CCCs for corrosion protection of aluminium alloys, are hybrid sol-gel coatings [4], which were investigated in the present work.

The introduction describes properties of aluminium and aluminium alloys, corrosion of aluminium and aluminium alloys, and different ways of their corrosion protection.

1.1 Aluminium and aluminium alloys

The aluminium alloys are divided into two classes: wrought and cast alloys [6]. Wrought alloys are cast into ingots of large size, then re-processed by mechanical processing methods such as rolling, extrusion, etc, while cast alloys are cast into the desired shape and size which can minimize the extra reprocessing [6]. In this project, the wrought aluminium alloys are taken into consideration.

1.1.1 Designations of alloys

Nine series of wrought and cast aluminium alloys are designated, based on different alloys

elements (Table 1.1, Table 1.2). The designation consists of four digits code. The first digit represents the series and the other numbers indicate the variants in the alloy. The designation also includes the prefix 'AA' as the shortness of aluminium alloy. They are listed in the Table 1.1 and 1.2 [6,7].

Table 1.1. Designation and main alloying elements of wrought aluminium alloys.

Designation of wrought alloy	Main alloying elements
AA1xxx	Pure aluminium (at least 99 wt%)
AA2xxx	Copper
AA3xxx	Manganese
AA4xxx	Silicon
AA5xxx	Magnesium
AA6xxx	Magnesium and silicon
AA7xxx	Zinc
AA8xxx	Lithium, iron or tin
AA9xxx	None (reserved for the future)

Table 1.2. Designation and main alloying elements of cast aluminium alloys

Designation of cast alloy	Main alloying elements
AA1xx.x	Pure aluminium
AA2xx.x	Copper
AA3xx.x	Silicon, copper and magnesium
AA4xx.x	Silicon
AA5xx.x	Magnesium
AA6xx.x	Unused alloys
AA7xx.x	Zinc
AA8xx.x	Tin
AA9xx.x	Unused alloys

For more information about the aluminium alloys, the temper designations are connected to the four-digit code, by a hyphen. It represents the heat or mechanical treatments the alloys have been through. The temper designation consists of a capital letter indicating the general type of treatment and a digit to specifying the treatment class. The temper designations of aluminium alloys are listed in Table 1.3 [6,7,8].

Table 1.3. Temper designation of aluminium alloys

Designation of temper	Description
H	Strain hardened
T	Aging heat treatment
O	Annealed
F	As-fabricated

Aluminium alloys used in the aerospace industry are usually from series AA2xxx, rich in copper, and AA7xxx, rich in zinc and magnesium, for example, AA2024-T3 and AA7075-T6. In this thesis, only AA2024-T3 was studied.

1.1.2 Aluminium alloys 2024-T3

The alloying elements in AA2024-T3 such as copper, magnesium and silicon provide the high strength, high fatigue resistance and good tolerance to damage. Nevertheless, it is also the reason for its low corrosion resistance [10]. AA2024-T3 is extensively used in airplane manufactures, especially for the wing and fuselage structures loaded in tension [11]. The chemical composition is listed in Table 1.4

Table 1.4. Chemical composition of commercial AA2024-T3 aluminum alloy [12]

Chemical Composition (wt%)									
Si	Fe	Cu	Mn	Mg	Cr	Ti	Zn	Others	Al
0.5	0.5	3.8-4.9	0.3-0.9	1.2-1.8	0.1	0.15	0.25	0.15	Rest

The results are obtained by electron probe microanalysis (EPMA) [14]. It is observed that there are a large amount of intermetallic particles (IMPs) in AA2024-T3. The IMs are distributed very heterogeneously. A more local observation of microstructure is shown in Fig 1.1. The composition of different phases and the corresponding colors are shown in Table 1.5.
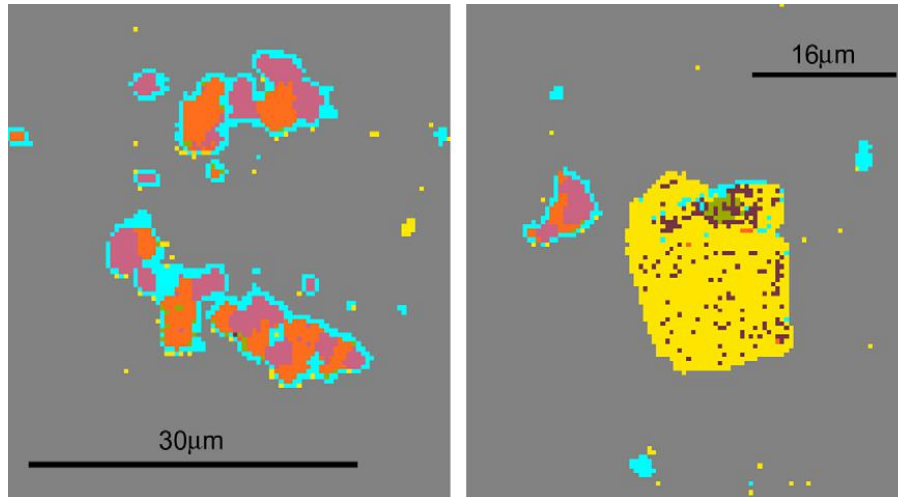
Figure 1.1. The local EPMA mapping of AA2024-T3. [14]

Table 1.5. Chemical composition and corresponding colors of phases in commercial AA2024-T3 [14]

Phase	Color	Al (%)	Cu (%)	Mg (%)	Mn (%)	Fe (%)	Si (%)
Al matrix	Grey	96	2	1	0	0	0
$Al_{20}(Cu,Fe,Mn)_5Si(Al_8Fe_2Si)$	Yellow	77	5	0	5	10	4
Al_2CuMg (S-phase)	Mauve	61	20	15	0	0	0
Al_2Cu (θ-phase)	Orange	70	27	0	0	0	0
$Al_{10}(Cu, Mg)$	Green	90	7	2	0	0	0
$Al_3(Cu,Fe,Mn)$	Brown	73	11	0	4	10	1
Periphery	Cyan	81	12	4	0	0	0

In some past researches, it is suggested that the S-phase is homogeneous. [15]. It can be seen that the composition of different phase particles varies considerably. The periphery phase is a Al-rich phase with higher content of Fe and Mn that that of S-phase and θ-phase, but still less than 1% [14]. The variety and distribution of IMs in AA2024-T3 is the reason why it has so many good properties compared to the pure aluminium. But the different potentials of different IMPs compared to the Al matrix cause the corrosion reaction. Some IMPs have low potentials (e.g. $MgZn_2$) which could dissolve fast and act as anodic sites [7]. Some IMPs have high potentials (e.g. Al_2Cu) which could sustain a large cathodic current, while some IMPs (e.g. Al_2CuMg) could switch from anodic sites to cathodic sites

during the corrosion with the Mg element dissolving. [9,15].

1.1.3 Corrosion of aluminium and aluminium alloys

Corrosion is a natural phenomenon leading to substantial material degradation even failure due to the chemical, biochemical and/or electrochemical interactions between a material and its working environment [6]. There are three types of corrosion to be considered [16].

- Wet corrosion: The material corrodes in the aqueous solutions or moisture by dissolving species.

- Dry corrosion: The material corrodes in a dry gaseous environment, usually in the high temperature environment.

- Non aqueous corrosion: The material corrodes in the non-aqueous environment, such as soils, molten salts.

In this thesis, the corrosion refers to the wet corrosion.

The corrosion of aluminium is conducted by the two half electrochemical reactions which are oxidation and reduction. During the corrosion Al is oxidized into Al^{3+} by releasing three free electrons (Equation 1.1) and oxygen is reduced with the electrons released by oxidation process to generate some new species in the electrolyte (OH$^-$)(Equation 1.2). Usually, the reduction reaction is the reduction of oxygen taking place in a mild alkaline aqueous environment as shown in Equation 1.2. The combination of oxidation and reduction makes the overall corrosion reaction (Equation 1.3) The aluminium ions are transformed into aluminium hydroxide by combining with the hydroxide ions [17,18].

- Oxidation: $$Al(s) \rightarrow Al^{3+}(aq) + 3e^- \qquad (1.1)$$

- Reduction: $$O_2(g) + 2H_2O(l) + 4e^- \rightarrow 4OH^- \qquad (1.2)$$

- Overall reaction: $$4Al(s) + 3O_2(g) + 6H_2O(l) \rightarrow 4Al(OH)_3(s) \qquad (1.3)$$
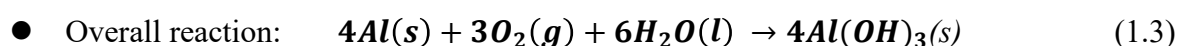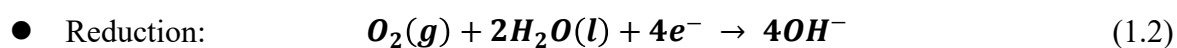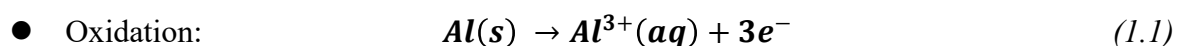
According to the different environments, the reduction reactions are different. The two key factors affecting the reduction reactions are the concentration of oxygen and pH of the solution. As shown in Equation 1.4, 1.5, 1.6 and 1.7, there are four different reduction reactions could take place at cathodic site. In the real situation, different cathodic reactions could take place at the same time due to the local differences of the solution when the solution is neutral (pH≈7) [16, 17].

- pH < 7 with no O_2: $$2H^+(aq) + 2e^- \rightarrow H_2(g) \qquad (1.4)$$

- pH < 7 with O_2: $$4H^+(aq) + 4e^- + O_2(g) \rightarrow 2H_2O \qquad (1.5)$$

- pH ≥ 7 with no O_2: $$2H_2O + 2e^- \rightarrow 2OH^-(aq) + H_2(g) \qquad (1.6)$$

- pH ≥ 7 with O_2: $$2H_2O + 4e^- + O_2 \rightarrow 4OH^-(aq) \qquad (1.7)$$
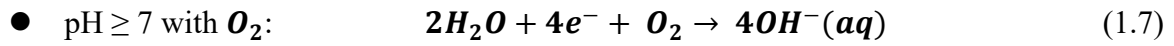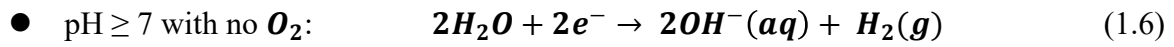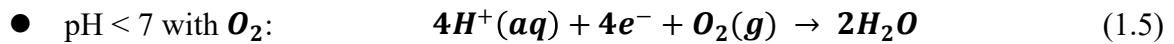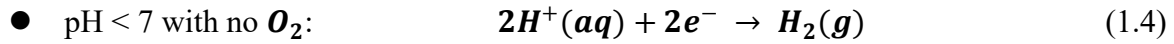
1.1.4 Passivation of aluminium

Aluminium is able to resist corrosion under moderately corrosive aqueous environment by naturally forming a thin protective oxide layer of alumina (Al_2O_3). The thickness of film is typically about 3 to 6 nm [18]. The formation of the alumina layer indicates the passivity of the aluminium alloy. The Pourbaix diagram is used for determining the possible equilibrium phases in an aqueous electrochemical system. It depends not only on pH and potential, but also on the temperature, pressure and concentration [18]. As shown in the Pourbaix diagram in Figure 1.2, the range of the passivation phenomenon is observed conveniently. Generally, when the potential is above -2.0 V, the passive layer Al_2O_3 is formed if the pH of its working conditions is between 4.0 to 8.5. In the strong acidic environment (pH<4.0), aluminium is corroded as in a form of Al^{3+}, while in the strong alkaline environment (pH>8.5), the aluminium is corroded into AlO_2^- [19]. When the potential is below -2.0 V, the aluminium alloys are in the immunity zone which can be protected in the pH range from -2 to 12.5.

However, the lines (a) and (b) correspond to water stability and its decomposed product. However, the alloying elements, temperature of environment, types of electrolyte (such as Cl^-), the corrosion rate and mode are not taken into consideration in Pourbaix diagram. The general principle of corrosion process is that by absorbing the aggressive ions (such as Cl^-), the passivation layer is locally damaged. Then some soluble transition complexes are formed with some cations on the surface of aluminium alloys [20]. Due to the complexity of the overall corrosion process, the mechanism of the damage caused by chloride ion (Cl^-) to the uniform passivation layer still needs further investigation [21].
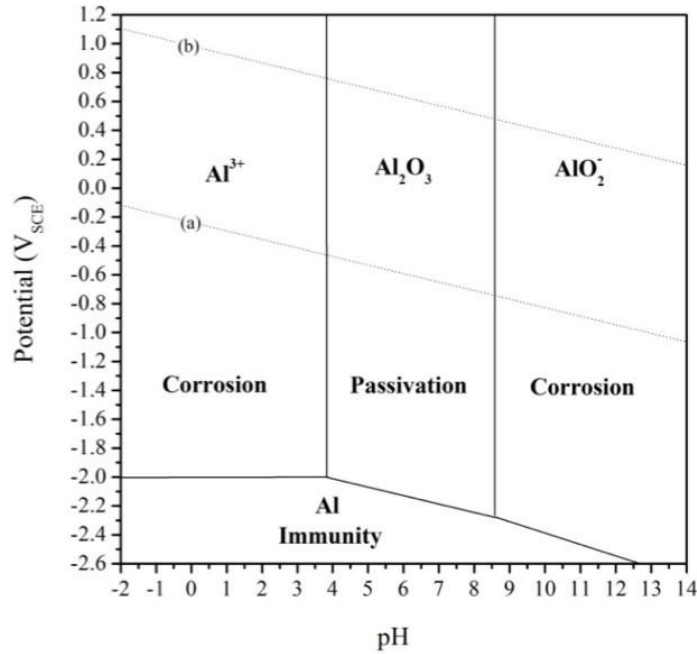
Figure 1.2. E-pH diagram for pure Al at 25 °C in aqueous solution [22].

The aluminium ions (Al^{3+}) reacts with oxygen ions or hydroxide ions from the dissociation of water to form the passivation layer (Al_2O_3) when the pH range of environment is from 4.0 to 8.5. The overall equation of this reaction is shown in Equation 1.8.:

$$2Al(s) + 3H_2O(l) \rightarrow Al_2O_3(s) + 6H^+ + 6e^-$$ （1.8）
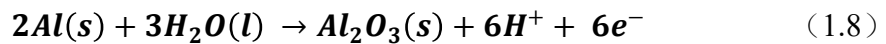
1.1.5 Types of corrosion

There are mainly two kinds of corrosion of aluminium alloys: (1) uniform corrosion, (2) localized corrosion.

The uniform corrosion of aluminium alloys often takes place when the aluminium alloys are loaded in the strong alkaline or acidic environment. The passivation layer (Al_2O_3) would be dissolved. The rate of the dissolution is faster than the formation of the Al_2O_3. The uniform corrosion is obvious that it can be measured by the loss of mass or the amount of hydrogen has been released [23,24].

In applications, the localized corrosion is more dangerous than uniform corrosion since we cannot notice it fast. But the localized corrosion could compromise the mechanical properties of aluminium alloys' structures.

14

The main types of localized corrosion of AA2024-T3 are pitting, galvanic corrosion and intercrystalline corrosion.

Pitting corrosion

Aluminium alloys are corroded by pitting corrosion when the service condition is neutral or near neutral, such as NaCl solution. The corrosion products $Al(OH)_3$ formed on the surface of alloys are gelatinous and white which can be observed. Pitting corrosion of aluminium alloy is shown in Figure 1.3.

The pitting corrosion have two stages which are initiation stage and propagation stage. In the initiation stage, the aggressive chloride ions (Cl^-) are absorbed on the oxide surface [24]. There are some complexes formed on the surface which lead to the thinning of passivation film (Al_2O_3). The breakdown of the passivation film leads to the propagation of pitting corrosion [25]. The fresh aluminium matrix is in contact with the electrolyte, leading the pitting goes further and deeper.
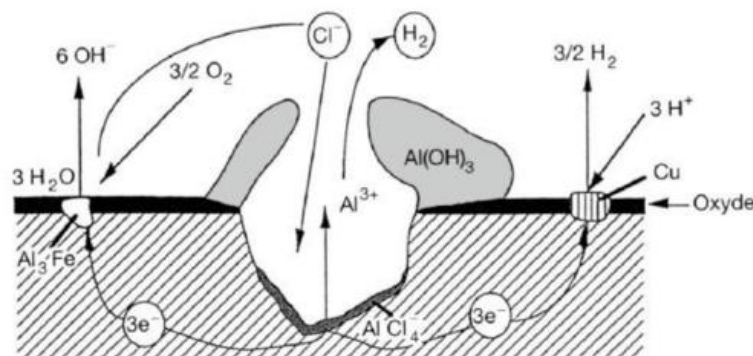
Figure 1.3. Pitting corrosion of aluminium alloy in sodium chloride. [23]

Galvanic corrosion

Since AA2024-T3 consists different intermetallic particles, the difference in electrochemical potentials between intermetallic particles and between intermetallic particles and matrix is present, resulting in electrochemical reaction (galvanic corrosion). IMPs with electrochemical potential more positive than matrix is local cathode (Cu) and with more negative is local anode (Zn). There are lots of micro galvanic couples formed between the matrix and IMs leading to the localized corrosion. This type of corrosion is called galvanic corrosion shown in Figure 1.4.
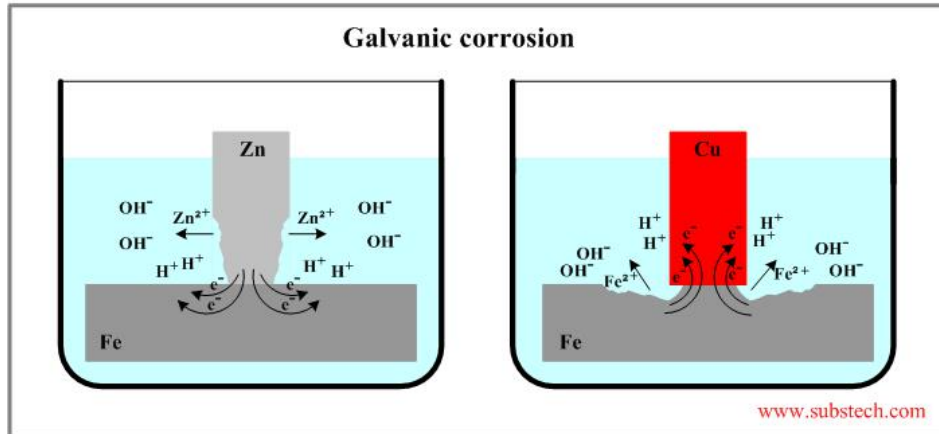
Figure 1.4. Schematic of galvanic corrosion between different elements [7].

According to Figure 1.4, the matrix-Al surrounding the particles acts local anode, due to the lower potential compared to the intermetallic particle (θ-phase) in (a) and (b). In (c) and (d), the intermetallic particle (S-phase) acts as anode and dissolves because its potential of magnesium is lower than the potential of matrix-Al. As the corrosion process progresses, either intermetallic particles or the matrix around are dissolved to form pits, resulting in pitting corrosion. The pits can cause stress concentration and lead to the cracks which compromise the safety of structures of aircrafts [26].

1.2 Corrosion protection scheme of aluminium and aluminium alloys

The common corrosion protection coating system used in aerospace industry requires high quality and the manufacturing process. Not only corrosion protection, but also the adhesion of the coating to the surface, aesthetics and integrity of structures are taken into consideration [27]. A typical coating system can be separated into 3 basic layers which are topcoat, primer and pretreatment, as shown in Figure 1.5.
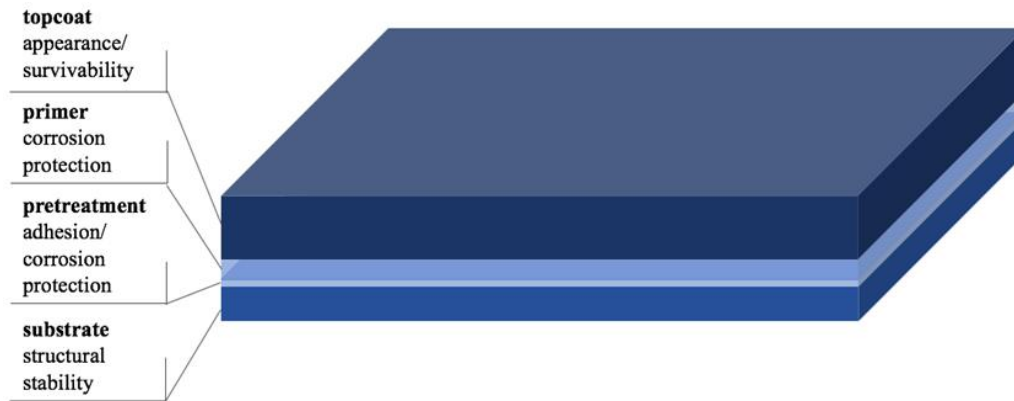
Figure 1.5. Schematic of 3 layers for the coating system in aerospace industry. [28]

Barrier properties of the coatings are usually related to some specific permeable materials, such as molecules of gases, electrolytes, liquids. They layer provide the barrier properties can prevent the mass transport of specific permeable materials through the thin layer [29]. The topcoat (Polyurethane and epoxy paints) provides the main barrier properties against the aggressive environments and decoration for the structures. Friction and abrasion properties are also from the topcoat layer. The thickness of top layer is from 25 to 150 μm. The primer layer is the main layer to provide corrosion protection. The typical primer layer includes inhibitive pigments which are soluble salts with some binders (e.g. SiO_2 nanoparticles) which are some continuous film-forming components and extenders which can increase the volume of coatings and provide good mechanical properties [30]. The pre-treatment is used for cleaning the oxides and contaminations on the surface. Then the primer layer could be bonded with the substrate better. Different pre-treatments also depend on different coating layers and are usually inorganic based [30].

In the present work, we focused on corrosion protection part/primer part.

Chromate conversion coatings (CCCs) have been used for corrosion protection of aluminium alloys over 100 years [31]. However, they are toxic and highly harmful to the environment and to human health. From 2006, their use was banned inform the European Union, by the Restriction of Hazardous Substances (RoHS) Directive 2002/95/EC, exceptions can only be made in defense and aerospace industries [32]. Thus, many replacements for CCCs have been proposed by the researchers worldwide, but their corrosion performances still not reached the performance of CCCs [33].

Based on the advantages such as low cost, simple synthesis procedures and easy adaption to applications in the manufacturing, sol gel coating technology emerges as one of the most promising alternatives for the CCCs [34].

17

1.2.1 Hybrid sol gel coatings

The synthesis of the sol-gel solution is shown in Figure 1.6. The precursors are chosen to be mixed together in the solution to form bonds through the chemical reactions. The first step is to form a sol, which is a stable liquid containing colloidal particles suspended homogenously [35]. In the sol, during the stirring of solution, a strong network named gel is formed. When it is applied on the surface of aluminium alloys by dipping or spraying, after curing at certain temperature for a certain period of time, the gel becomes more rigid and robust.
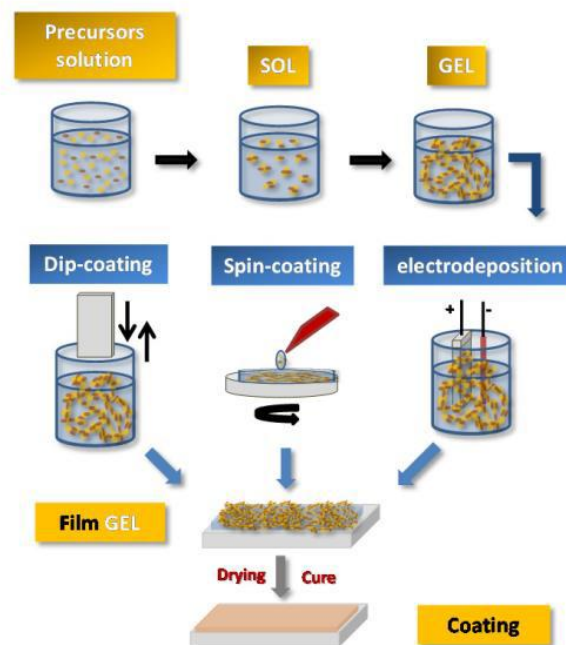
Figure 1.6. Different stages of sol gel coating synthesis [36].

At the beginning of the research in the sol gel coating technology, precursors used for sol gel coatings are inorganic because of the good mechanical properties provided by them. It can also improve the adhesion between alloy surface and the coating [37]. But so many microcracks inside the coating compromise the corrosion protection performance. Then the idea to combine inorganic and organic precursors together is further investigated and performs well during the corrosion. The organic precursors which has three methoxy groups and an epoxy ring provide flexibility of the coatings and the mechanical support is from the inorganic ones [35, 36, 38].

The bonding among the precursors within the sol gel coatings are classified into three classes:

- Class I: the organic and inorganic precursors connect through hydrogen bonds, Van der Waals forces, ionic bonds.

- Class II: the organic and inorganic precursors connect through covalent bonds, the network is provided by the condensation of gel precursors

- Class III: the organic and inorganic precursors connect through both types of bonds in class I and class II.

In this project, the organic-inorganic hybrid (OIH) sol gel coating is based on the class II, which is appropriate for the corrosion protection of aluminium alloys.

There are two main stages in the synthesis of OIH sol gel coatings which are hydrolysis of metal alkoxides and polycondensation of hydroxyl groups [36,39]. In hydrolysis, the alkoxide groups are replaced by the hydroxyl groups in an aqueous solution. The gel network is made by the polycondensation process in which the hydroxyl groups condense into new water molecules. Then the M-O-M bonds are formed in the sol-gel coatings. It is shown in the Figure 1.7. M is the matrix element, such as Si, Ti, Zr. R represents the alkyl groups, R^* is a symbol of a carbon chain with some other function groups.
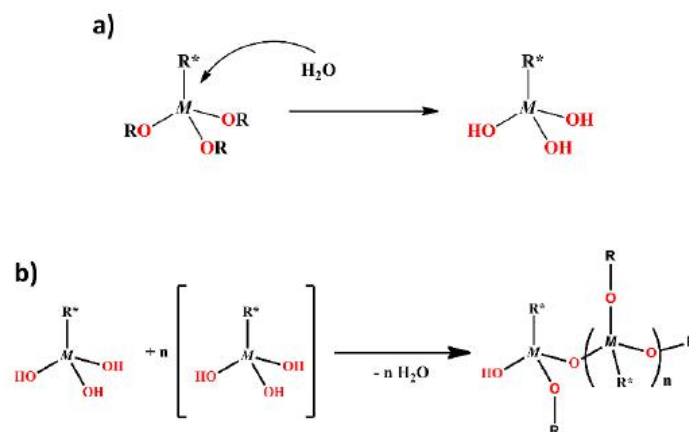
Figure 1.7. The hydrolysis and polycondensation of the precursors [39].

There are many kinds of precursors used for synthesis of OIH sol gel coatings for corrosion protection of metals, the main elements composed of them are carbon oxygen and silicon. Some of them are listed in Table 1.6.

Among precursors listed in Table 1.6, the inorganic alkoxisilane, TEOS and organic GPTMS are the most common precursors used for corrosion protection of aluminium alloys [4]. As shown in Figure 1.8, the proportions of TEOS and GPTMS of all the publications for aluminium alloys are 46% and 72% separately.
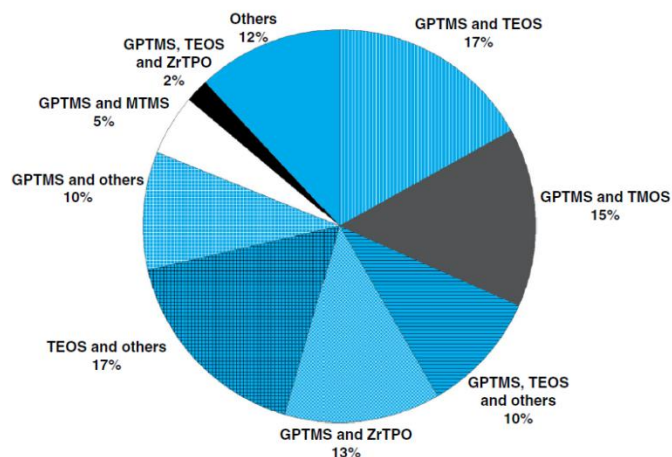
Figure 1.8. Precursors for synthesis of sol gel coating for aluminium alloys [4].

Various studies confirmed barrier properties of hybrid sol-gel coatings which are a result of polymerization between organic and inorganic precoursors [4,40]. Furthermore, a stable M-O-Si bonding is formed between the sol-gel and the passivation layer of metal substrate. In this project, the layer is aluminium oxide (Al_2O_3), and the bonding is Al-O-Si as shown in Fig 1.9.
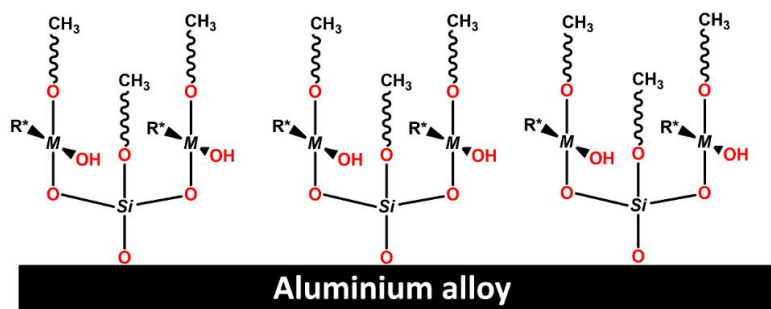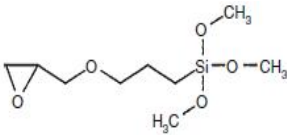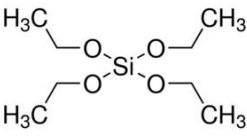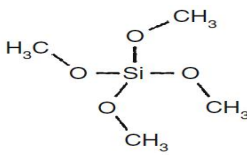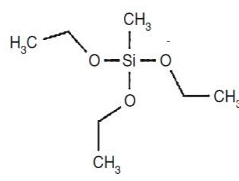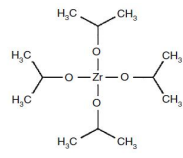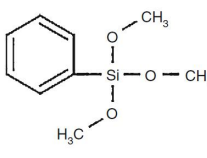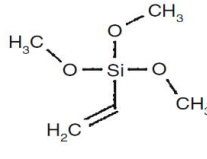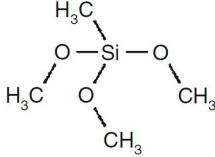
Figure 1.9. Schematic of interactions between coatings and metal surface [41].

However, to achieve an active corrosion protection, corrosion inhibitors should be added to the coating [41].

Table 1.6. Some of the commonly used precursors for synthesis of OIH sol gel coatings [4].

Chemical name	Abbreviation	Empirical formula	Structure
3-**G**lycidoxy**p**ropyl-**tri**methoxy**si**lane	GPTMS	$C_9H_{20}O_5Si$	
Tetra**eth**ox**y**silane	TEOS	$C_8H_{20}O_4Si$	
Tetra**m**ethyl**or**tho**si**licate	TMOS	$C_4H_{12}O_4Si$	
Methyl**tri**eth**oxy**silane	MTES	$C_7H_{18}O_3Si$	
Zir**c**onium(IV) **t**etra-1-**pr**op**o**xide	ZrTPO	$C_{12}H_{28}O_4Zr$	
Phenyl**tri**m**eth**oxy**si**lane	PTMS	$C_9H_{14}O_3Si$	
Vinyl**tri**m**eth**oxy**si**lane	VTMS	$C_5H_{12}O_3Si$	
Methyl**tri**m**eth**oxysilane	MTMS	$C_4H_{12}O_3Si$	

1.2.2 Inhibitors

To enhance active corrosion protection, corrosion inhibitors can be incorporated into the sol-gel coatings. Corrosion inhibitors are dispersed in the prime layer and react with the underlying substrate to prevent the corrosion propagate [42].

There are two types of inhibitors, organic and inorganic, which to minimize the corrosion rate in the aqueous environment of aluminium and aluminium alloys [6,7, 42, 43]. The classification of inhibitors is summarized below:

- Organic inhibitor: It works as both anodic and cathodic inhibitors to suppress the half-cell reactions mainly by absorption to generate a layer to separate the substrate from the aggressive environment. for example: amines, thiourea.

- Inorganic inhibitor: It generally reduce the kinetics of anodic and cathodic reactions.

  - Anodic inhibitor: It reacts with the metal ions released from the anodic sites to form an insoluble film. This film can reduce anodic dissolution rate. For example, nitrite.

  - Cathodic inhibitor: The metal ions deposit on the substrate surface to block the cathodic reactions and prevent the migration of reducible ions. For example, rare earth salts such as cerium salts.

  - Mixed inhibitor: The inhibitor which can work on the anodic sites and cathodic sites.

In reality, the inhibitors that work both on anodic and cathodic sites also exist, for example: chromate [44].

In this project, inhibitors based on cerium and lithium salts were studied, where the cerium based inhibitor works as cathodic inhibitor and the lithium base inhibitor works as anodic inhibitor.

1.2.3 Coating with lithium as inhibitor

Among all the corrosion protection methods mentioned above, the coating with lithium ions as inhibitor is a promising replacement for CCCs [45]. Especially in alkaline environment, it can prevent the aluminium alloys from corrosion. A lot of researches has

found that the lithium is able to insert into the $Al(OH)_3$ and stabilize the passivation layer formed on the surface [45,46,47,48]. According to the results from Buchheit et al, during the corrosion of Al-Cu-Li aluminium alloys, there is a Al-Li layered double hydroxide (LDH) being formed [47]. It covers the exposed area of samples to provide the corrosion protection. The composition of this LDH is $MII(1-x)MIII(x)(OH)2[An-]x/n$ [48].

Based on the researches above, the lithium containing coating has been investigated further. It has been found that the lithium can act as leaching inhibitor to provide active corrosion protection for aluminium alloys [46,47,48].

As shown in Figure 1.10, the formation of this protective layer is divided into three main stages. In stage I, Al_2O_3 layer is stable when the pH range from 4 to 9 [49]. When the pH is around 10, the Al_2O_3 layer start to be thinned with the absorption of Cl^- [48]. When the Al_2O_3 layer is broke, the stage II starts. The aluminium alloys start to dissolve and form $Al(OH)_3$ layer on the substrate surface. Since this environment is alkaline, the $Al(OH)_3$ transform into $Al(OH)_4^-$. The transformation of $Al(OH)_3$ layer can lead to more dissolution of substrate. The formation of the $Al(OH)_3$ gel contribute to the increase of OCP. In stage III, the dissolution and growth of the layer both exist. Li also intercalate into the $Al(OH)_3$ gel to form the layer double hydroxide (LDH) in stage III [50]. The OCP will increase continuously in this stage III until the competition between dissolution and growth of the layer become stable.
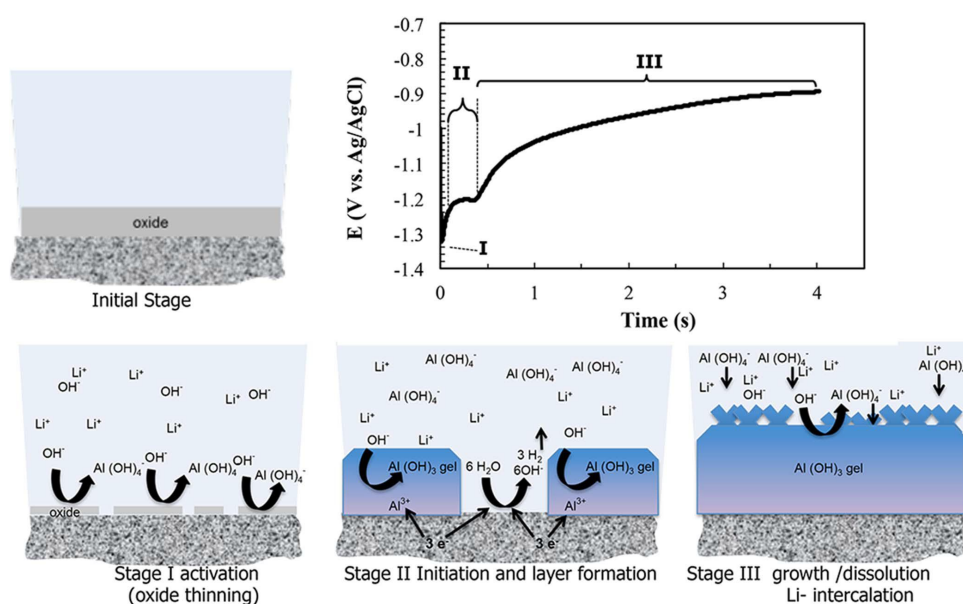
Figure 1.10. Schematic illustration of the formation of protective layer [48]

23

1.2.4 Coating with cerium as inhibitor

The soluble rare-earth salts have been found can act as cathodic inhibitors [31,42,54]. The deposition of these salts could block the cathodic reaction then prevent the corrosion propagation. It is also a new alternative method for CCCs [52]. The cerium has been studied extensively and has good effect of corrosion inhibition [54,55].

The Ce^{3+} in the coating with be oxidized into Ce^{4+} with the help of O_2 at the interface of electrolyte and aluminium alloy [53]. The process of Ce corrosion inhibition process is illustrated in Figure 1.11. When corrosion reaction starts, reduction of oxygen occurring at the cathodic sites produces lots of hydroxide ions (OH⁻). It leads to the pH rise in the solution. When the pH rise to about 10, The Ce^{3+} would leach out from the coating and react with the OH⁻ into $Ce(OH)_3$. The $Ce(OH)_3$ precipitates at the cathodic sites and is oxidized into $Ce(OH)_4$. The $Ce(OH)_3$ can migrate to the damaged area and then also precipitate as $Ce(OH)_4$ and CeO_2 [55]. $Ce(OH)_4$ and CeO_2 which deposited at the cathodic sites are not soluble. They can act as a protective barrier against the oxygen and lower the corrosion process. Moreover, the addition of Ce^{3+} as an inhibitor into the sol gel coating can also provide self-healing effect [54, 55, 56].
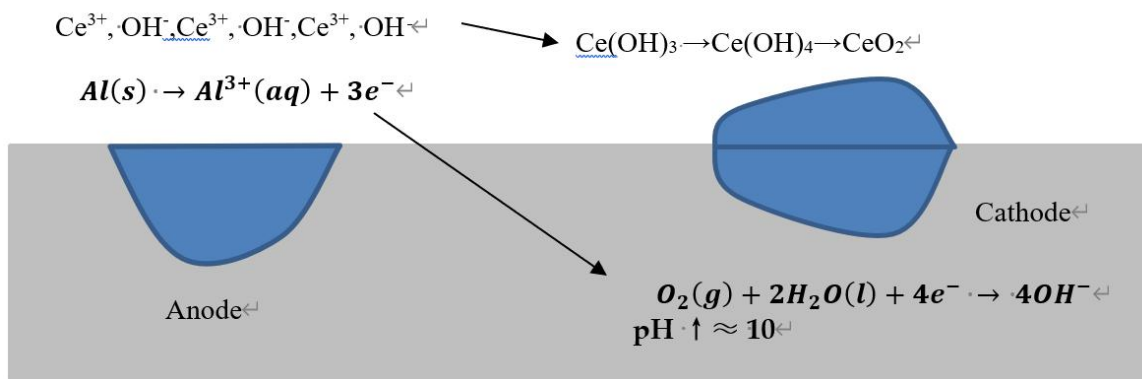
Figure 1.11. Schematic of mechanism of cerium inhibitors

1.3 Objectives of the project

The aim of this project is to investigate the corrosion protection of lithium and cerium based inhibitors when they are incorporated into the hybrid sol-gel coatings, which are applied on AA2024-T3. The hybrid sol-gel coatings were based on GPTMS and TEOS. The lithium salts used in this project are lithium hydroxide (LiOH), lithium nitrate (LiNO$_3$). Cerium salt used in this project is cerium nitrate hexahydrate Ce(NO$_3$)$_3$·6H$_2$O. Concentration of cerium salt was previously optimized [47,77], while the concentration of lithium salts studied in this work is also based on previous researches. An active corrosion protection of Li and Ce salt was studied with the following techniques: potentiodynamic polarization measurements, electrochemical impedance spectroscopy (EIS), immersion test and digital optical microscopy. Finally, the synergistic effect of Ce and Li was studied. To decrease costs of the synthesis of sol-gel coating, the optimal curing temperature for synthesis is needed [ref]. The lower temperature of curing, the lower cost of the synthesis. Thus, the effect of different curing temperatures on corrosion resistance of sol-gel coating was also investigated.

Electrochemical techniques including potentiodynamic polarization measurement and electrochemical impedance spectroscopy (EIS) analysis were used to investigate the anti-corrosion properties, mechanism and inhibition effect of these two inhibitors. Digital microscopy was used to observe the morphology of the scribed coatings applied on AA2024-T3 after different days of immersion.

2   Methods

Electrochemical measurements are necessary for the assessment of corrosion performance for different materials. There are several electrochemical measurements, such as Open circuit potential (OCP), Linear polarization resistance (LPR), Tafel plot extrapolation (TP) and Electrochemical impedance spectroscopy (EIS). Since the corrosion process is complex, it requires two or more measurements to characterize the corrosion performance. With the results of the measurements, the service life of the materials during the applications can be predicted [57]. All the electrochemical measurements mentioned above are based on the typical three-electrode cell which has the material for testing as working electrode, the Ag/AgCl or calomel electrode as the reference electrode, whose potential is constant, and the platinum plate as the counter electrode to complete the circuit. Three-electrode cell is shown in Figure 2.1.
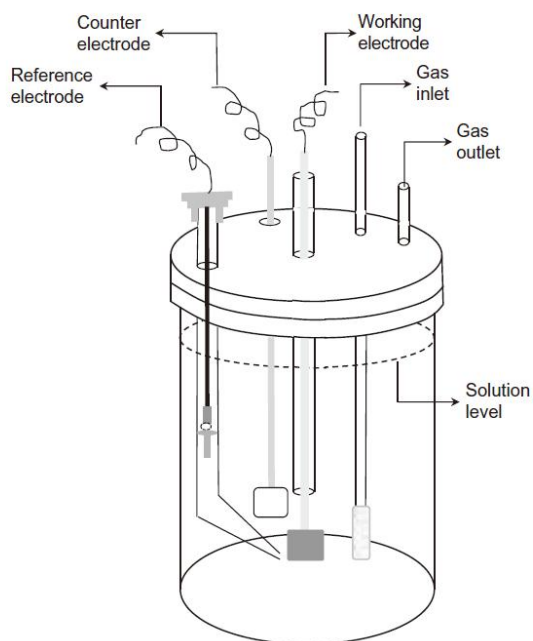
Figure 2.1. A three-electrode cell for electrochemical measurements [58].

Open Circuit Potential (OCP)

The Open Circuit Potential (E_{OCP}) measurement is usually used as pre-processing for electrochemical measurements [59]. There is no current passing the electrode and no potential applied on the electrodes during this measurement. The difference between working electrode and reference electrode is measured. It can measure the equilibrium of

the system thermodynamically. Usually the system can be regarded as stable or stable enough when the variety of potential vs. time is within ± 5mV [58]. The variety of E_{OCP} is recorded by monitoring the E_{OCP} vs. time. E_{OCP} is a reference potential for further measurements, such as linear polarization resistance (LPR) and potentiodynamic polarization measurements.

Tafel Plot extrapolation (TP)

When the potential is far away (about 300mV) from the corrosion potential, the cathodic and anodic reactions are both depend on transfer of the electronic charges. They can be represented by the Tafel slope for anode and cathode as β_a and β_c respectively.

The Tafel Plot extrapolation is conducted on the surface of sample about 300 mV directed to positive and negative potential with respect to the corrosion potential [58]. The corrosion potential is determined by the Open Circuit technique before the polarization measurement.

The principle of the potentiodynamic polarization measurements is based on the Bulter-Volmer Model which is described by the Bulter-Volmer equation.

The Butler-Volmer Model is established based on the electrochemical kinetics by John Alfred Valentine Butler and Max Volmer. It is used to describe the polarization by the equation shown below:

$$i = i_0 \{ \frac{C_o(0,t)}{C_o(\infty,t)} exp\left[\frac{\alpha zF\eta}{RT}\right] - \frac{C_R(0,t)}{C_R(\infty,t)} exp\left[-\frac{(1-\alpha)zF\eta}{RT}\right] \}$$

If the solution is stirred enough and distributed homogenously, the limitation of mass transfer by convection can be ignored. So all the C_O (x, t) and C_R (x, t) terms can be ignored. The equation can be simplified to the classical Butler-Volmer equation [61]:

$$i = i_0 \{ exp\left[\frac{\alpha zF\eta}{RT}\right] - exp\left[-\frac{(1-\alpha)zF\eta}{RT}\right] \}$$

i: current density

i_0: exchange current density

F: Faraday constant

R: gas constant

η: overpotential

T: absolute temperature

α: anodic charge transfer coefficient

z: number of electrons transferred in the reaction

C_O (x, t): the time-dependent concentration of the species to be oxidized

C_R (x, t): the time-dependent concentration of the species to be reduced

The Tafel Plot extrapolation can determine the corrosion rate and corrosion potential directly. It can be used to predict the corrosion properties for different corrosion systems with good accuracy. And it can also be used to measure extremely small corrosion rates [62]. During Tafel method, the testing materials are usually polarized 150-300mV below and above the OCP [59]. The voltage step is between 5 to 10 mV for most cases. The Tafel slope for both anode (β_a) and cathode (β_c) can be determined by the tangent in the linear zones of the polarization curve. The intersection of the tangent of both cathodic and anodic curves is the determined value of corrosion potential and current [62]. It is shown in Fig 2.2.
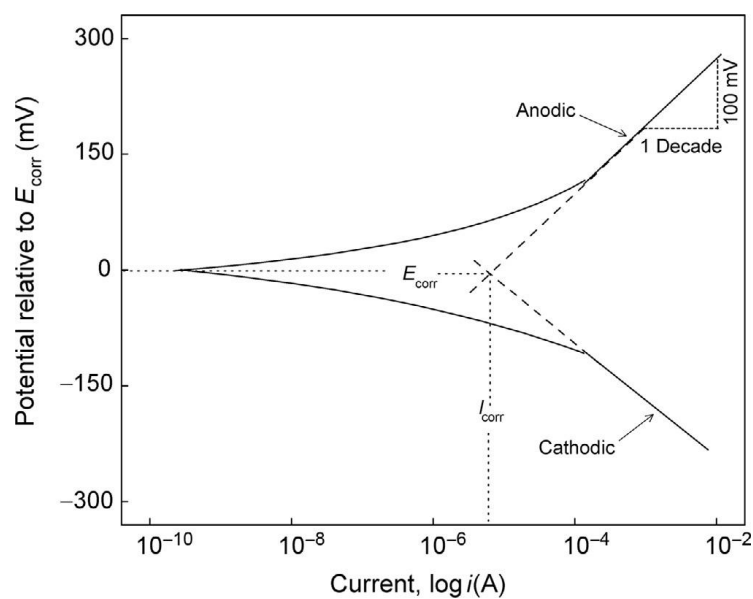
Figure 2.2. The typical Tafel plot extrapolation. [58]

The equation for Tafel plot is related to the electrochemical reaction rate and the overpotential. When the overpotential is large enough, the Butler-Volmer equation transforms into the form as equation shown below.

$$i_c = i^0 exp \frac{-\alpha_c F \eta}{RT}$$

The Tafel approximation shows that the potential of metals is related to the equivalent current for a single reaction on the surface [62]. When applying the equation of $a_c = 2.3 \left(\frac{RT}{\alpha_c nF}\right) log i^0$ and $b_c = -2.3 \left(\frac{RT}{\alpha_c nF}\right)$ in the equation above, it becomes:

$$\eta = b_c log \frac{i}{i^0}$$

η: overpotential

b_c: Tafel slope

i: current density, A/m^2

i^0: exchange current density, A/m^2

Electrochemical Impedance Spectroscopy (EIS)

The Electrochemical Impedance Spectroscopy (EIS) is essential for the investigation of corrosion process of complex interfaces during the immersion time [58]. The corrosion reaction at the interface is characterized by a circuit composed of resistors and capacitors in EIS. It can determine the parameters for corrosion properties of the interface such as resistance (R_p) and capacitance (C_d). It is efficient in the analysis of inhibitor performance, passivation of metals and barrier properties of coatings [63,64].

EIS is conducted by the 'single-sine' method. The different frequencies can be measured successively or by multisine implementation that measure all frequencies at the same time, but a further Fourier transformation is needed [65]. A small sinusoidal amplitude of AC excitation is applied to the three-electrode cell system and the response in the frequency range of 10 mHz to 100kHz is recorded and studied as shown in Fig.2.3. The time shift is due to the slow response of the whole system.
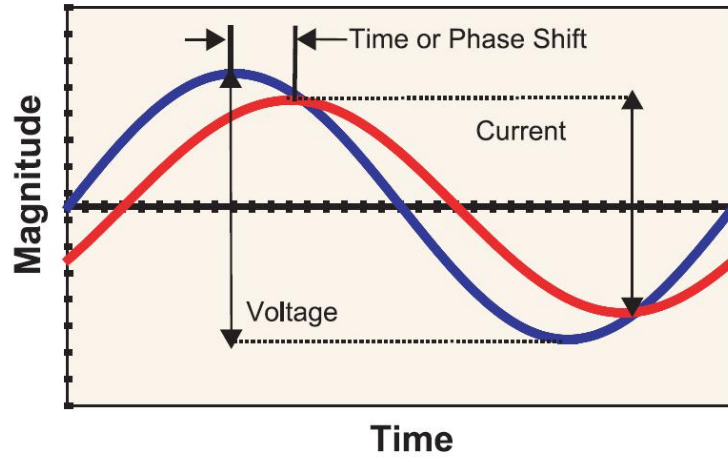
Figure 2.3. Sinusoidal potential and current signal as the function of time. [66]

The data obtained by EIS can be used to characterized the properties of interface and construct an equivalent circuit model to investigate the structures of interface and the reactions taking place at the interface. Commonly, a very small AC excitation signal is used to measure the impedance. The response to the three-electrode cell is pseudo-linear. In the pseudo-linear system, the corresponding current for the sinusoidal potential signal is also sinusoidal but with a shifted phase but the same frequency [66]. The necessary equations are listed below:

$$E_t = E_0 \sin(\omega t)$$

$$I_t = I_0 \sin(\omega t + \emptyset)$$

By Eulers relationship,

$$\exp(j\emptyset) = \cos(\emptyset) + j sin(\emptyset)$$

Based on Ohm's law,

$$Z_\omega = \frac{V}{I} = Z_0 \exp(j\emptyset) = Z_0(\cos(\emptyset) + j sin(\emptyset))$$

E_t: the input voltage

E_0 the voltage amplitude

I_t: the output current

I_0: the current amplitude

$$\Phi: \text{shift angle of phase}$$

$$Z_\omega: \text{the impedance composed of complex number}$$

E_t is the excitation signal and the I_t is the response. With the equation mention above, the impedance of the system can be calculated.

The results of EIS can be expressed as two plots which are Bode plots and Nyquist plot.

The Nyquist plot is plotted with the impedance data measured at different frequencies. The impedance is composed of imaginary part and real part, as shown in Figure 2.4. The imaginary part of impedance is along the Y-axis and the real part is on the X-axis. The intersection of the curve with the X-axis at low frequency gives us the information about the total resistance of polarization and solution ($R_\Omega + R_p$). While at high frequency, only the solution resistance can be obtained.
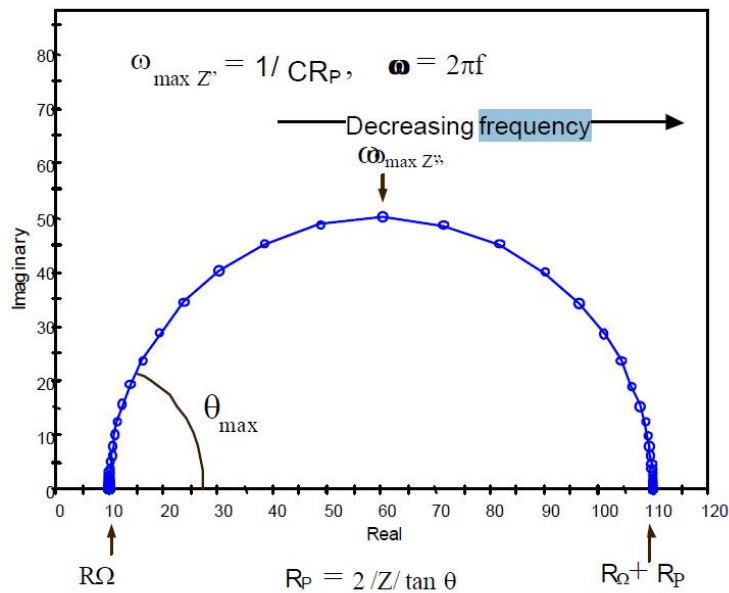
Figure 2.4. Nyquist plot and the corresponding equivalent circuit. [68]

Another representation of the EIS is Bode plot in which the log $|Z|$ and phase angle $\emptyset$ are plotted vs. log (Hz), as shown in Figure 2.5. The impedance at the high frequency range represent the properties of the outer interface which is the interface between coating and solution [67]. The impedance at the intermediate frequency indicate the properties inside of the coating which is the oxidation layer between the substrate and coatings. The corrosion resistance at the interface of inner metal and coating can be determined by the impedance at low frequency [55]. The value of the impedance Z from the Bode plot at the

frequency of 0.01 Hz can be used to determine the corrosion resistance [68]. Higher phase angle and impedance, at low frequency part, indicate better corrosion protection of the system [67].
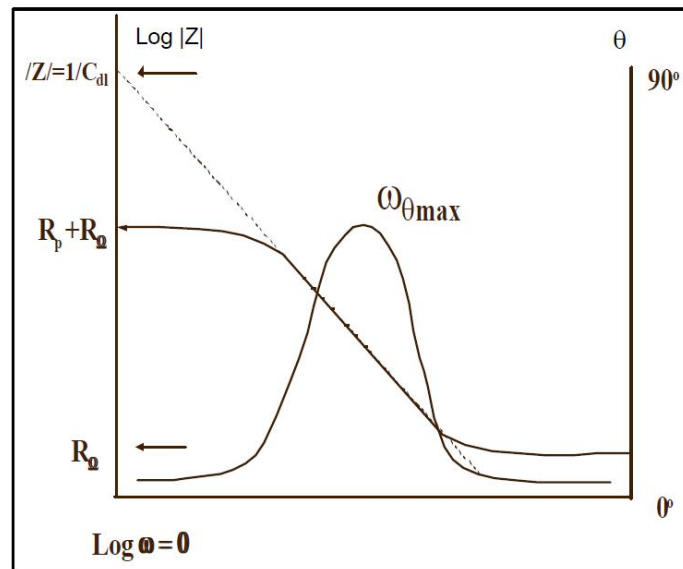
Figure 2.5. Bode plot for a corrosion system. [68]

3 Experimental

All electrochemical measurements were conducted in 0.1 M NaCl electrolyte. The scribed samples were immersed in 0.5 M NaCl electrolyte to accelerate the corrosion process. The materials, techniques and synthesis for sol gel solution with different inhibitors are listed and described below.

3.1 Materials preparation

The material used in this thesis is AA2024-T3, with the dimensions of 40mm × 40mm × 2mm. Samples were sanded by the sandpaper in the sequence of # 320 grit, # 800 grit, # 1200 grit, # 2000 grit. Then all sanded samples were immersed in the ethanol and clean it in Ultrasonic cleaning machine for 10 minutes and dry with the air gun.

To investigate the active corrosion protection of the lithium and cerium as corrosion inhibitor, the cross shaped scribes were made by ceramic knife manually (Fig. 3.1). The depth of the scribe is assumed to be bigger than the depth of the coating.
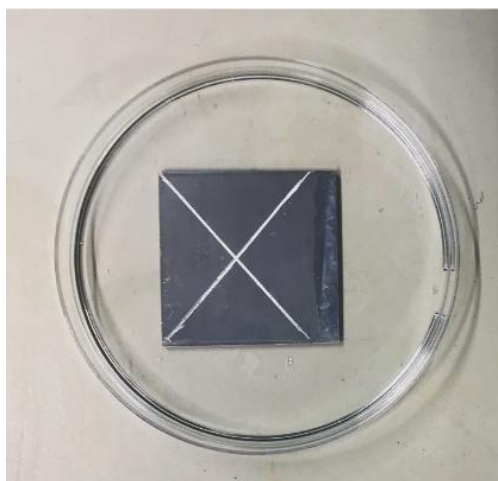
Figure 3.1. The scribed samples for immersion and EIS

3.2 Sol-gel synthesis and deposition

Seven hybrid sols were prepared, one undoped and others with different inhibitors of different concentration.

The first sol was without any inhibitor and labelled as GTS. It was prepared by mixing the 3-(glycidyloxypropyl) trimethoxy silane (GPTMS, Aldrich, 98%), Tetraethyl orthosilicate

(TEOS, Aldrich, 98%) and a colloidal silica (SiO_2) nanoparticle suspension (Ludox-4S, Aldrich, aqueous suspension 40 wt%, particle size 9 nm, pH 9). After 30 minutes of stirring, 0.3 mL of concentration nitric acid (HNO_3, KMG, 69.5%) was added into 50 g of solution as a catalyst. The absolute ethanol (EtOH, Honeywell, 99.8%) was added as a dissolvent. 10 more minutes of stirring was needed after the addition of HNO_3 and EtOH. The molar ratio of the GTS was $GPTMS/TEOS/SiO_2 = 0.5/0.5/0.54$.

The second sol was labelled as GTS-$LiNO_3$-3%. It was prepared in the same steps as mentioned above, but including lithium as a corrosion inhibitor. The GPTMS and TEOS and major part of EtOH were added together and stirred for 30 minutes. Lithium nitrate ($LiNO_3$, Alfa Aesar, 99.8%) was added to another small amount of EtOH separately and stirred for 15 minutes. After that, they were added together before the addition of catalyst HNO_3. Another 10 minutes of stirring was needed after the addition of HNO_3. The molar ratio of the GTS-$LiNO_3$-3% was $GPTMS/TEOS/SiO_2/LiNO_3 = 0.5/0.5/0.54/0.03$.

The third sol was labelled as GTS-LiOH-3%. It was prepared in the same process as discussed above. The inhibitor was lithium hydroxide (LiOH, sigma-Aldrich, 98%) instead of $LiNO_3$. The stirring process of the LiOH with the EtOH needs the extra Ultrasonic process for 10 minutes to increase the dissolution of LiOH. The molar ratio of the GTS-LiOH-3% was $GPTMS/TEOS/SiO_2/LiNO_3 = 0.5/0.5/0.54/0.03$

The fourth and fifth sols were labelled as GTS-$LiNO_3$-1% and GTS-$LiNO_3$-5%. They were prepared in the same steps as GTS-$LiNO_3$-3%, only changing the molar ratio of $LiNO_3$ from 3% to 1% and 5%.

The sixth sol was labelled as GTS-Ce. The inhibitor was cerium nitrate ($Ce(NO_3)_3·6H_2O$, Aldrich, 99%). It followed the same process as the synthesis of GTS-$LiNO_3$. The molar ratio of the GTS-Ce was $GPTMS/TEOS/SiO_2/ Ce(NO_3)_3·6H_2O = 0.5/0.5/0.54/0.03$.

The last sol was labelled as GTS-Li-Ce. It was prepared in the same steps as mentioned above, but including both lithium and cerium as corrosion inhibitors. Lithium nitrate ($LiNO_3$, Alfa Aesar, 99.8%) and cerium nitrate ($Ce(NO_3)_3 · 6H_2O$, Aldrich, 99%) were adding to small amount of EtOH separately and stirring for 15 minutes. It was added before the catalyst HNO_3. The molar ratio of the GTS-Li-Ce was $GPTMS/TEOS/SiO_2/LiNO_3/ Ce(NO_3)_3·6H_2O = 0.5/0.5/0.54/0.015/0.015$.

After the preparation of different sols, they were deposited on the AA2024-T3 substrate by dip-coating technique, with a withdrawal rate of 30 cm/min. Finally, the samples with

coatings were cured in the oven, from 20 ℃ to 120 ℃ with the ramp of 5 ℃/min, then curing for 1h, and cool down from 120 ℃ to 20 ℃ with the same ramp.

3.3   Experimental settings

All electrochemical experiments conducted on the samples were immersed in 0.1 M NaCl solution at room temperature. All samples were placed into the three-electrode cells with an exposed area of 1 cm^2. The three-electrode cell was connected with CSP-300 of Bio-Logic multichannel potentiostat and controlled by the EC-Lab software. The coated AA2024-T3 sample is working electrode (red), the silver /silver chloride (Ag/AgCl, 3M KCl) is reference electrode (white, 0.192V vs. standard hydrogen electrode) and the platinum is counter electrode (blue). The electrochemical cell set up is shown as Fig 3.2.
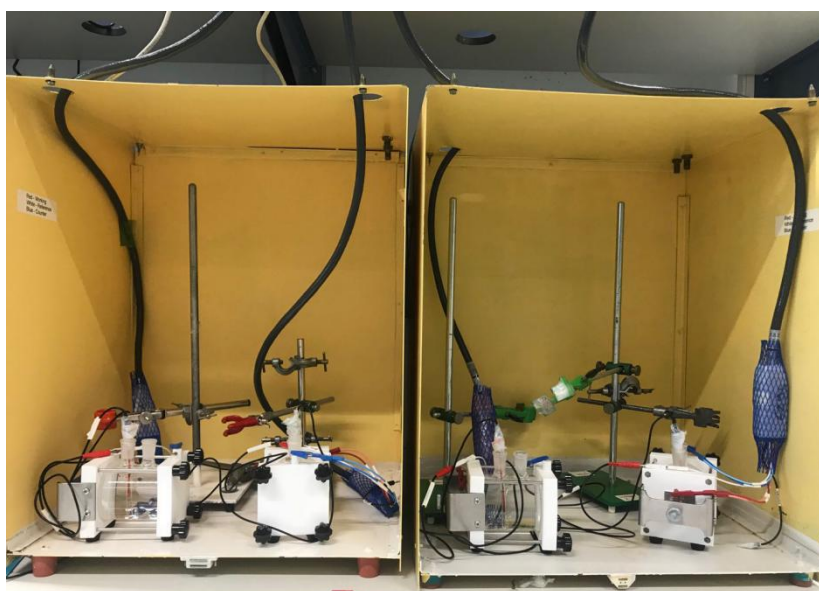
Figure 3.2. The electrochemical cell set up for measurements

The work was divided into two parts. In the first part we evaluated the corrosion protection of intact coatings by potentiodynamic polarization measurements and electrochemical impedance spectroscopy (EIS). In the second part, the active corrosion protection and self-healing ability of scribed coatings.

3.3.1 Evaluation of intact coatings

The corrosion performance of the intact coatings was evaluated by potentiodynamic polarization measurements and electrochemical impedance spectroscopy (EIS). Before all the electrochemical measurements, 1h of Open Circuit potential (OCP) was carried out to stabilize the system.

Potentiodynamic polarization measurement

The potentiodynamic polarization measurement scanned the surface of sample from -250 mV to E_{OCP} and E_{OCP} to 1 V at a scanning rate of 1 mV/s separately. It was repeated three times and the most representative result was chosen for plotting.

Electrochemical impedance spectroscopy (EIS)

The EIS measurements are performed in a frequency range from 10^{-2} to 10^5 Hz with excitation voltage of 10mV sinusoidal amplitude, for 28 days. The corrosion resistance is evaluated by analyzing the modulus of impedance module Z from the Bode plot (Z vs. f) at low frequency of 0.1 Hz. EIS of each intact coating was repeated three times and the most representative result was chosen for plotting. The deviation bar was added in the plot of modulus of impedance at 0.1 Hz vs time (days) by using the data from all three times measurements.

Effect of curing temperature

To investigate the effect of curing temperature on the sol-gel coating corrosion resistance GTS was cured at the following temperatures: room temperature (20°C), 60°C, 80°C, 100°C and 120°C. Samples cured at room temperature were kept in the box for 24h to obtain the formation of intact coating. Other samples were cured in the same oven as mentioned above from 20°C to each peak temperature separately with a ramp of 5°C/min, then curing for 1h, and cool down from each peak temperature to 20 °C with the same ramp and then stored in the box for 24 hours to get the same conditions as for the room cured samples. EIS of all differently cured samples were measured after 1hour of OCP. All settings and parameters for EIS were the same as discussed above. Measurements were repeated three times and the most representative result was chosen for plotting. The deviation bar was added in the plot of modulus of impedance at 0.01 Hz vs temperature by using the data from all three times measurements.

3.3.2 Evaluation of scribed coatings

To study an active corrosion protection of the lithium and cerium nitrates as corrosion inhibitor, the samples with the cross shaped scribes were evaluated by the immersion test and electrochemical impedance spectroscopy (EIS). 1h of Open Circuit Potential (OCP) was carried out before the EIS experiment.

Immersion test

The immersion test was carried out in the 0.5 M NaCl aqueous solution for 7 days, at room temperature to monitor the corrosion process of the scribe. The 0.5 M NaCl aqueous solution was dripped on the surface of the samples to ensure all the area of scribes are immersed. Digital optical microscopy (Keyence VHX-100) with 18 mega-pixel CCD camera was used to observe the morphology of the scribes for various immersion time to analyze the corrosion process. The magnification was kept constant which is 200X.

Electrochemical impedance spectroscopy (EIS)

The EIS measurements were performed in 0.1 M NaCl, in a frequency range from 10^{-2} to 10^5 Hz with excitation voltage of 10mV sinusoidal amplitude, for 14 days. Before the EIS measurements scribed samples were immersed in the 0.5 M NaCl solution for 48 hours to accelerate the corrosion process. The corrosion resistance is evaluated by analyzing the modulus of impedance Z from the Bode plot (Z vs. f) at low frequency of 0.01 Hz. Measurements were repeated three times and the most representative result was chosen for plotting. The deviation bar was added in the plot of modulus of impedance at 0.01 Hz vs time (days) by using all the data from all three times measurements.

4   Results and Discussion

The study was divided into two parts (i) corrosion behavior of intact coatings including results of potentiodynamic polarization measurement and EIS measurements and (ii) corrosion behavior of scribed coatings including the results of immersion test and EIS measurements.

4.1 Corrosion behavior of intact coatings

Potentiodynamic polarization measurement

Potentiodynamic polarization measurements were conducted to analyze the corrosion inhibiting effect of different corrosion inhibitors on the anodic and cathodic reactions. Figure 4.1 summarized all the polarization curves after 1h OCP of the uncoated AA2024-T3 samples and coated with different sol-gel coatings. There are three repetitions for each one of the different coatings. The corresponding electrochemical parameters obtained from the polarization curves are listed in Table 4.1, where we chose the most representative curve for calculation. The corrosion currents and potentials are determined by the tangent of the cathodic and anodic curves in the linear region about $\pm$ 20 mV (vs. E_{corr}). as shown in Table 4.1. The Figure 4.2 present the comparison of all representative polarization curves for different sol gel coatings. The effect of different concentrations of lithium nitrates on sol gel coatings is also measured, it is shown in the appendix (Figure 1, 2).

The curve of substrate AA2024-T3 shows immediate dissolution when anodically polarized vs. the OCP and the cathodic curve is limited by diffusion [47]. The polarization curves of the samples with different coatings demonstrate the inhibiting effect of the corrosion inhibitors obviously. The corrosion currents of the samples that were exposed to the sol gel solutions were suppressed by at least about an order of magnitude compared to the values of substrate AA2024-T3.

The corrosion potentials of samples with GTS and LiOH coatings were shifted to more noble values about -0.7 V (vs. AgCl) as shown in Fig 4.1. The cathodic currents of these samples were reduced by an order of magnitude. The corrosion current of GTS coating is 0.024 μA while the corrosion current of LiOH coating is 0.005 μA. The passive range of GTS coating indicates good barrier properties. The GTS and GTS-LiOH-3% coatings

demonstrated clear passive ranges at the anodic branches. The passive range of GTS-LiOH-3% coating is about 0.4V compared to 0.24V of the samples with GTS coatings The addition of LiOH shows wider passive range compared to that of the GTS coatings which means better barrier properties. It shows the LiOH is a good cathodic inhibitor.

However, the corrosion potential of samples with GTS-LiNO$_3$-3% coatings shifted to a positive value compared to substrate AA2024-T3. The shape of the curves of substrate AA2024-T3 and GTS-LiNO$_3$-3% coating remains similar which indicate the GTS-LiNO$_3$-3% coating had poor barrier properties. The GTS-LiNO$_3$-3% coating reduced the corrosion current to 0.008 μA with no obvious passive ranges at anodic branch. The protective layer formed with Li ions is composed of 3 separate layers which are columnar layer, porous layer and barrier layers [69]. This Al-Li layered double hydroxide (LDH) is porous which has poor barrier properties [46-48]. It shows the LiNO$_3$ is a good anodic inhibitor.

Due to the presence of lithium and cerium as corrosion inhibitors, the corrosion currents of samples with GTS-LiNO$_3$-3% and GTS-Ce coatings were smaller than that of samples of GTS coatings. The corrosion potential of GTS-Ce coatings was reduced slightly to about -0.6 V compared to that of substrate AA2024-T3. The passive range of GTS-Ce coating is about 0.1 V which is clearly larger than that of the substrate AA2024-T3. The corrosion current is 0.003 μA which is the lowest corrosion current compared to all the sol gel coatings. The cathodic current was suppressed by an order of magnitude, leading to the slowing down of the whole corrosion process and provide a good corrosion protection. It is accomplished by the formation of protective layer of CeO$_2$ against the oxygen at cathodic sites to lower the rate of reduction reaction and then lower the rate of whole corrosion process [54-56]. The Ce(NO$_3$)$_3$ acts as a cathodic inhibitor.

To avoid the precipitation, when we study the combination of lithium salts and cerium salts, we keep the anion the same which is NO$_3^-$ in this thesis. Thus, even if LiOH-3% showed a promising result on corrosion protection, LiNO$_3$ is our choice to study further.
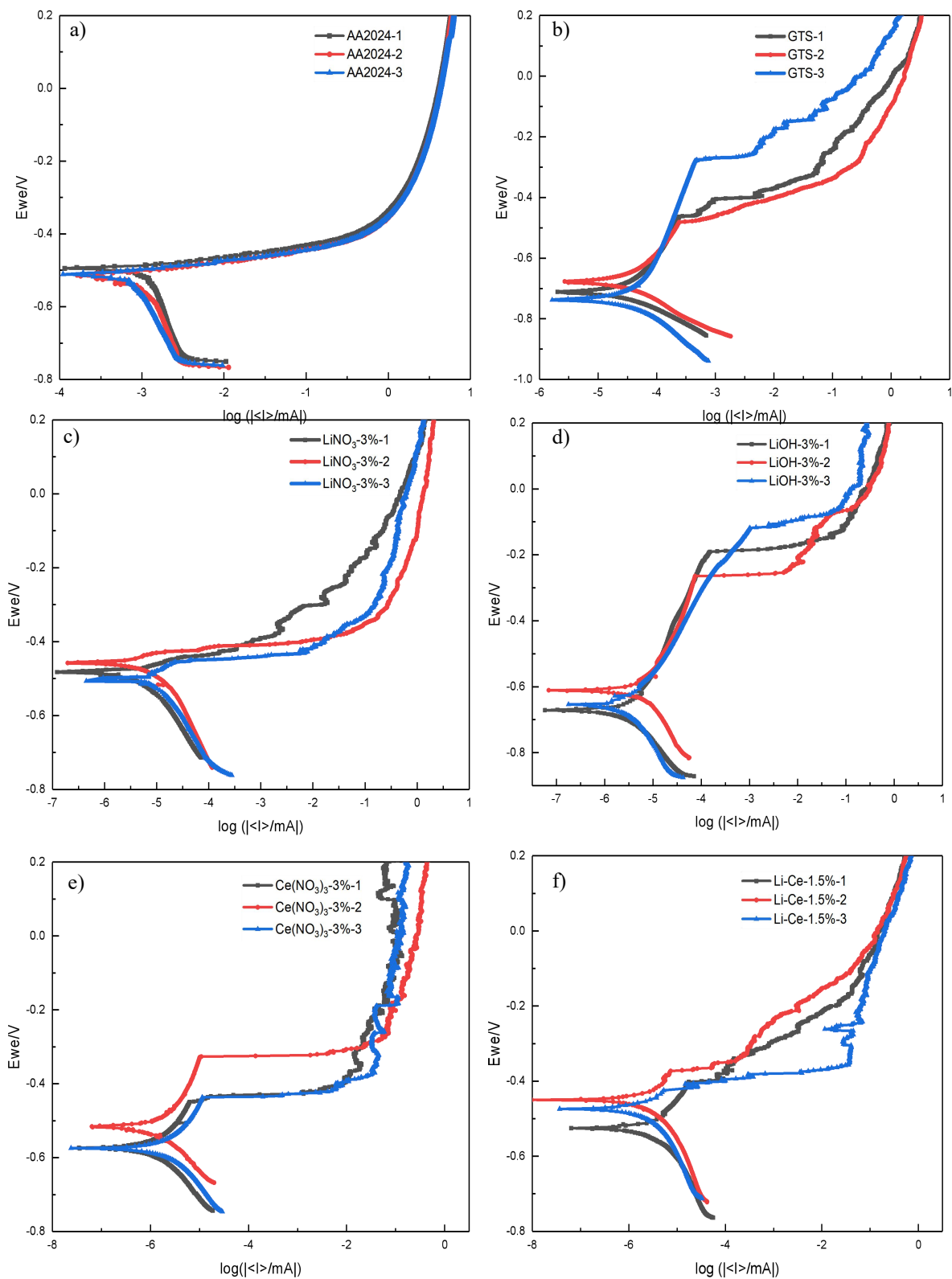
Fig 4.1. Potentiodynamic polarization curves for AA2024-T3 in 0.1M NaCl with and without corrosion inhibitor, a) AA2024-T3, b) GTS, c) GTS-LiNO$_3$-3%, d) GTS-LiOH-3%, e) GTS-Ce-3%, f) GTS-Li-Ce-1.5%
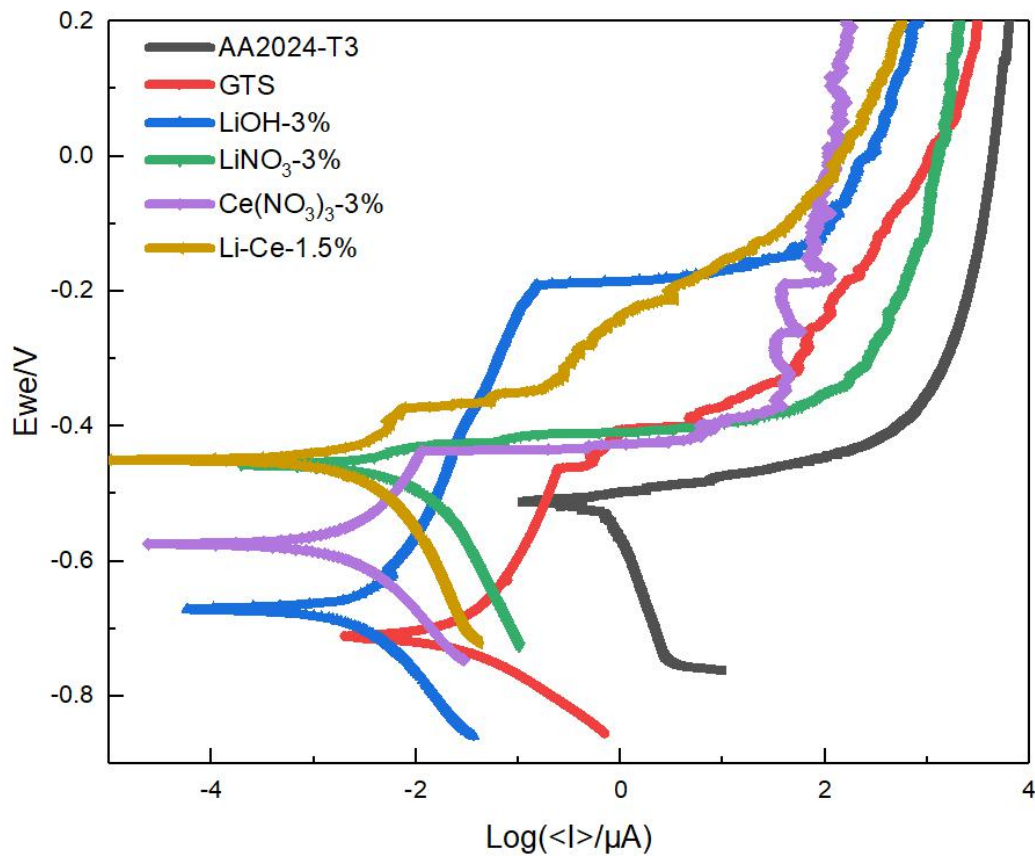
Figure.4.2. The polarization curves with different inhibitors and without inhibitors

Table 4.1. electrochemical parameters calculated from the potentiodynamic polarization curves in Fig 4.1.

Samples	E_{corr}/(mV vs. AgCl)	i_{corr} (μA)	β_a/mV	β_c/mV
AA2024-T3	-511±20	0.52±0.35	28±1	-173±30
GTS	-711±35	0.024±0.015	179±45	-92±15
LiNO$_3$-3%	-458±50	0.008±0.009	95±55	-165±50
LiOH-3%	-671±60	0.005±0.002	331±60	-297±85
Ce(NO$_3$)$_3$-3%	-574±60	0.003±0.002	229±40	189±20
Ce-Li -1.5%	-451±75	0.003±0.002	145±25	-148±40

The corrosion potential of the samples with GTS-Li-Ce coatings remains about -0.45 V (vs. AgCl) with respect to that of the samples with GTS-LiNO$_3$-3% coatings. Compared to the value of substrate AA2024-T3, it also shifted to the positive direction. Both the

cathodic and anodic currents are reduced, as shown in Figure 4.2. The passive range on the anodic curve of GTS-Li-Ce coatings is larger than that of the GTS-LiNO$_3$-3% coatings which indicate better barrier properties compared to bare AA2024-T3 and GTS-LiNO$_3$-3% coatings. It indicates the inhibition of the anodic activity or pitting [47,55]. The corrosion current of GTS-Li-Ce is 0.003 μA, the same as that of GTS-Ce coating. It is also the lowest corrosion current compared to all sol gel coatings.

The corrosion currents of the samples with different sol gel coatings were suppressed at least by an order of magnitude compared to the values of substrate AA2024-T3, as shown in Table 4.1 and Figure 4.2. The GTS coating, GTS-LiOH-3% coating and GTS-Ce coating show good barrier properties compared to AA2024-T3. The $Ce(NO_3)_3$ and LiOH act as the cathodic inhibitor while the LiNO$_3$ acts as the anodic inhibitor. The combination of LiNO$_3$ and $Ce(NO_3)_3$ acts as the mixed inhibitor.

The GTS-Li-Ce coating and GTS-Ce coating have the lowest corrosion current of 0.003 μA which means lowest corrosion rate of the coatings applied on the AA2024-T3. Since the corrosion potential of GTS-Li-Ce coating is more positive than that of GTS-Ce coating, it can be concluded that the GTS-Li-Ce coating is the best sol gel coating for AA2024-T3.

Electrochemical impedance spectroscopy (EIS)

The EIS measurements were used as a non-destructive testing method to analyze the electrochemical properties of different coating systems during the immersion time. The impedance modulus, |Z|, and the phase angle, φ, were plotted as the function of frequency, f, (Bode plots) for various coatings on AA2024-T3 for different time up to 28 days. The most representative results are shown in Figure 4.3 and discussed qualitatively in accordance with the previous work on the hybrid sol gel coatings on aluminium alloys [46-48, 54, 55]. The other two repetitions are plotted and listed in the appendix (Figure 3, 4). In general, high frequency range indicate the information of the coating/electrolyte interface, the intermediate frequency region was related to the oxide layer between coating and substrate. The low frequency region provided the information about the corrosion happened at the interface of the substrate and sol gel coatings [55,67].

AA2024-T3 coated with GTS expresses, two time constant, observed at frequency of 1 Hz and 10^5 Hz (Figure 4.3 a, b). The impedance modulus at the low frequency and intermediate frequency range was constantly decreasing with the time, which indicated the corrosion protection was compromised by the immersion in 0.1 M NaCl. After 3 days of immersion, the biggest decrease of impedance at low frequency is noticed. The maximum value of phase angles shifted to higher frequencies and the absolute values of phase angle at 0.01 Hz increased. The increase in the low frequency range (10^{-2}-10^{-1} Hz) indicated the deterioration in corrosion protection of coatings. This deterioration may be caused by the small cracks on the oxide layers which allow the migration of chloride ions [43, 45]. In high frequency range, the reduction of absolute value of the phase angles also indicated that the coating capacitance is decreasing with the immersion time.

AA2024-T3 coated with GTS-Ce-3% showed different corrosion behavior compared to the plots of GTS-Li-3% coatings (Figure 4.3 c, d). At low frequency range, the impedance modulus of GTS-Ce coatings was higher than that of GTS coatings which means higher corrosion resistance. The modulus of impedance at low frequency was decreasing with the time in accordance of the absolute value of phase angle is also decreasing while the maximum absolute value of phase angles shifted to higher frequencies, which indicated the lower corrosion resistance of the coating systems [55]. During the first week of immersion, the impedance module of GTS-Ce coatings was around 10^6 Ohm/cm^2, while the impedance of GTS coatings decreased to around 10^5 Ohm/cm^2 after 2 days of immersion. The biggest reduction of impedance for GTS-Ce-3% coatings was observed

after 14 days immersion while for GTS coatings it occurred after 3 days of immersion. So the GTS-Ce-3% coating is an improved coating compared to GTS coatings with a better corrosion protection.

AA2024-T3 coated with GTS-Li expresses two time constant, observed at frequency of 1 Hz and 10^5 Hz (Figure 4.3 e, f). The time constant at low frequency gives the information at the inner interface of oxide layer and substrate while the time constant at high frequency indicates the information at the out interface between oxide layer and electrolyte [42, 45]. The shapes of EIS spectra showed a more capacitive shape, an obvious linear range at the intermediate frequency during the first 4 days of immersion [55] compared to the curves of GTS-Ce-3% coatings at the same period. The impedance modulus at low frequency and intermediate frequency was decreasing along the immersion time. The largest impedance reduction occurred after 4 days of immersion. The value of impedance after 7 days of measurement was still above 10^5 Ohm/cm^2 which is way better than the impedance of GTS coatings at the same time, but was lower than the impedance of GTS-Ce-3% after 7 days of measurement. It shows that GTS-Li-3% coating is also a good coating for corrosion protection of AA2024-T3 compared to GTS coatings, but its performance is not as good as that of the GTS-Ce-3% coating.

Finally, AA2024-T3 coated with GTS-Li-Ce-1.5% also expresses two time constant, observed at frequency of 1 Hz and 10^5 Hz (Figure 4.3 g, h). The GTS-Li-Ce-1.5% coatings exhibited good corrosion protection compared to the 3 coatings discussed above. During the 3 days of immersion, the trend in the impedance vs. frequency plot was similar to that of the GTS-Li-3% coatings. The modulus of impedance at low frequency was above 10^6 Ohm/cm^2 in the first week, which means excellent corrosion protection. It better than all three coatings above, while after 7 days of measurements, the impedance of GTS coating was about 3.2×10^4 Ohm/cm^2, the impedance of GTS-Ce-3% coating is below 10^6 Ohm/cm^2 and that of GTS-Li-3% coating was about 10^5 Ohm/cm^2. The obvious reduction of impedance was observed after 10 days of measurement, which is also later than that of GTS coatings and GTS-Li-3% coatings. The absolute value of phase angle at low frequency decrease to the lowest value after 10 days immersion, then increased again. the absolute values of phase angle at 0.01 Hz increased which means corrosion protection of the protective layer formed with the help of lithium and cerium was compromised. The reduction of absolute value of phase angle at high frequency indicated the decline of the coating stability, which happened for all the coatings discussed above. Based on results in Figure 4.3, the GTS-Li-Ce-1.5% is the best sol gel coating among all the coatings.
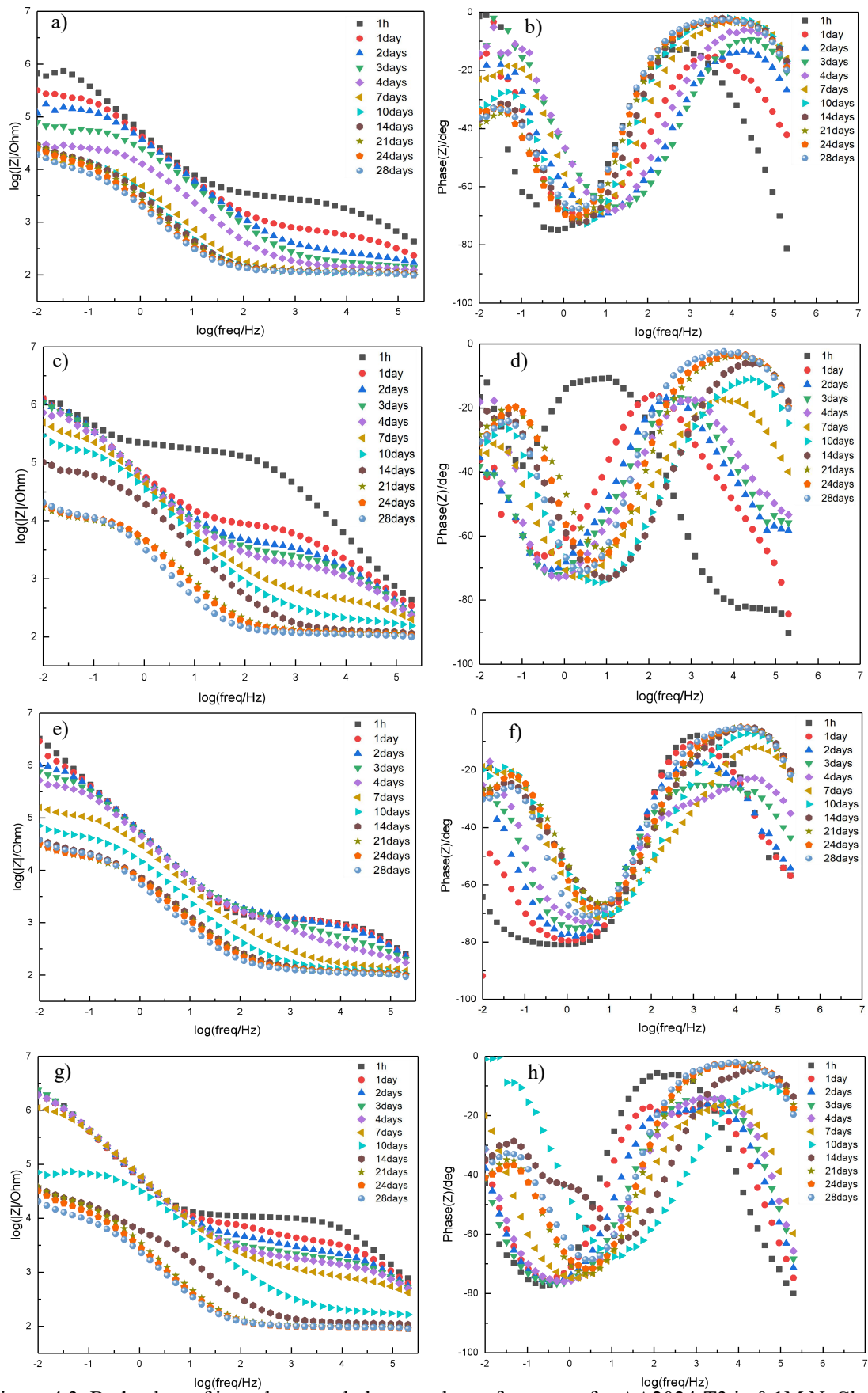
Figure 4.3. Bode plots of impedance and phase angle vs. frequency for AA2024-T3 in 0.1M NaCl with and without corrosion inhibitor for 28 days, (a, b) GTS, (c, d) GTS-Ce-3% (e, f) GTS-Li-3%, (g, h) GTS-Li-Ce-1.5%

The impedance value determined at 0.1 Hz in the Bode plot of modulus of impedance vs. frequency was chosen as the parameter representing the corrosion resistance of the coating [54,55]. Values of impedance of 0.1 Hz as a function of immersion time are presented for all coated samples, which is shown in Figure 4.4.

The $Z_{0.1}$Hz value of samples with GTS coatings decreased with time over the 28 days. At the beginning, the modulus of impedance is high due to its barrier properties. During the first 5 days of immersion, the impedance dropped evidently, showing the loosing of coating capacitance. This is due to the coating itself is porous, the chloride ions could migrate into the coating system and react with the substrate underlying the coatings [55]. After 7 days of measurements, the impedance decreased slowly up to 28 day of immersion.

The $Z_{0.1}$Hz value of samples with GTS-Li-3% coatings decreased with time. However, the addition of lithium as corrosion inhibitor slowed down the trend of impedance reduction compared to GTS. In the first 3 days, the values of impedance remained at a relatively high level, over 10^5 Ohm/cm^2, while the same time, the impedance of GTS samples dropped evidently. After 3 days immersion, the value of impedance started to decrease, the drop in the impedance module is observed. But the rate of impedance reduction is still slower than that of GTS coatings. After 16 days of immersion, the impedance decreased to a low value of $2x10^4$ Ohm/cm^2 and stayed steady.

The $Z_{0.1}$Hz value of samples with GTS-Ce-3% coatings decreased slower than that of GTS coatings and GTS-Li-3%. The impedance of GTS-Ce-3% coatings stayed over 10^5 Ohm/cm^2 for 14 days which is longer than that of the GTS coatings and GTS-Li-3% coatings. The protection by cerium as inhibitor is better than the protection of lithium as inhibitor. It may be explained that the Al-Li LDH formed on the surface is porous [46, 48], while the CeO$_2$ precipitated at the cathodic sites is intact and insoluble [55]

The $Z_{0.1}$Hz value of samples with GTS-Li-Ce-1.5% coatings remained above $3.2x10^5$ Ohm/cm^2 in the first week. At the same time, the impedance of the GTS, GTS-Li-3% and GTS-Ce-3% coatings were all decreasing to some extent. It means the GTS-Li-Ce-1.5% provide the best corrosion protection compared to all other 3 different coatings. After 7 days, the impedance of GTS-Li-Ce-1.5% coatings dropped clearly. The rate of the impedance reduction is faster than that of the GTS-Ce-3% and GTS-Li-3% coatings at the same period. After 16 days, there is an increase of impedance value which was not observed in other 3 coatings. It may be the result of the synergistic effect of cerium and lithium inhibitors.
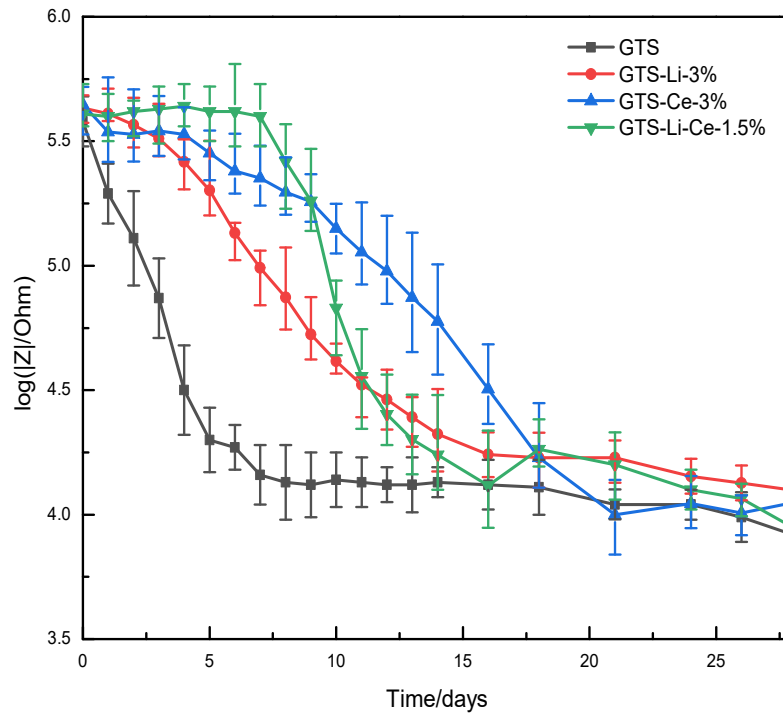
Figure 4.4. Values of $Z_{0.1Hz}$ (impedance at 0.1 Hz obtained from Bode plots in Figure 4.3, Figure 3 and 4 in the appendix) for different coatings on AA2024-T3 as a function of time in 0.1 M NaCl solution

Base on EIS results, all coatings with inhibitor show better anti-corrosion behavior compared to the GTS coatings, since they all stay at higher impedance value for a longer time and reduce slower than the GTS coatings. During the corrosion progression, the lithium could leach out and form the Al-Li LDH layer, while the cerium could also leach out to form the insoluble CeO_2 to slow down the rate of corrosion [46-48,54,55]. The GTS-Ce-3% coating show better protection than GTS-Li-3%, it may relate to that the protective layer formed by Li is porous [47]. The best protection was provided by the GTS-Li-Ce-1.5% coating because it stayed at the high value of impedance for the longest time and have a increase after 16 days of measurement.

Effect of temperature

The electrochemical characteristics of the GTS coatings under different curing temperatures were measured by EIS after 1h OCP. Figure 4.5 shows the Bode plots of the GTS coatings under different temperatures. Each temperature has been measured 3 times and the other two repetitions were shown in the appendix (Figure 5).

In Figure 4.5 a), the impedance modulus shows an increase of impedance values in the low frequency (10^{-2}-10^{-1} Hz) and intermediate frequency (10^1-10^3 Hz) with the curing temperature increasing. There is an exception of room temperature samples, which also showed higher value of impedance. With the increasing temperatures, the shapes of EIS spectra showed a more capacitive shape [55], an obvious linear range at the intermediate frequency (10^1-10^3 Hz).

The corresponding phase angle plots of the EIS measurements were shown in Figure 4.5 b). The maximum absolute value of phase angles shifted to lower frequencies and the absolute values of phase angle at 0.01 Hz increased. At 0.01 Hz, the sample cured at 120℃ has the highest absolute value of phase angle, the samples cured at room temperature and 60℃ had lower value of the phase angle. The increase in the low frequency range (10^{-2}-10^{-1} Hz) indicates the improvement in corrosion protection of coatings.
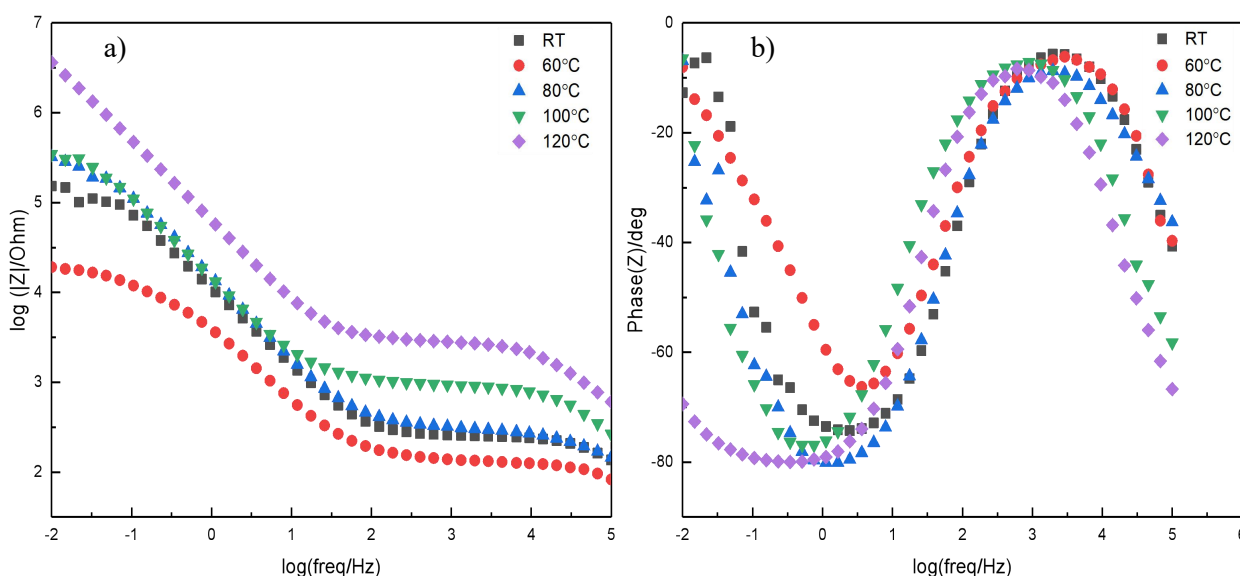
Figure 4.5. Bode plots of impedance and phase angle vs. frequency for AA2024-T3 in 0.1M NaCl without corrosion inhibitor of different curing temperatures.

The impedance modulus of GTS coatings of different curing temperatures at 0.01 Hz were chosen to plot the bar diagram to compare corrosion resistance of GTS after different curing temperature (Fig. 4.9). From 60 ℃ to 120 ℃ the impedance modulus increased with the increased temperature. Higher curing temperature might lead to higher degree of polycondensation which could provide better corrosion protection [38,41]. The impedance modulus of curing at room temperature also shows a relatively good corrosion protection, but it needs more investigation to verify the results.

Figure 4.6. Values of $Z_{0.01}$Hz (impedance at 0.01 Hz obtained from Bode plots in Fig 4.8) of differently cured GTS for different temperatures applied on AA2024-T3 in 0.1 M NaCl solution

4.2 corrosion behavior of scribed coatings
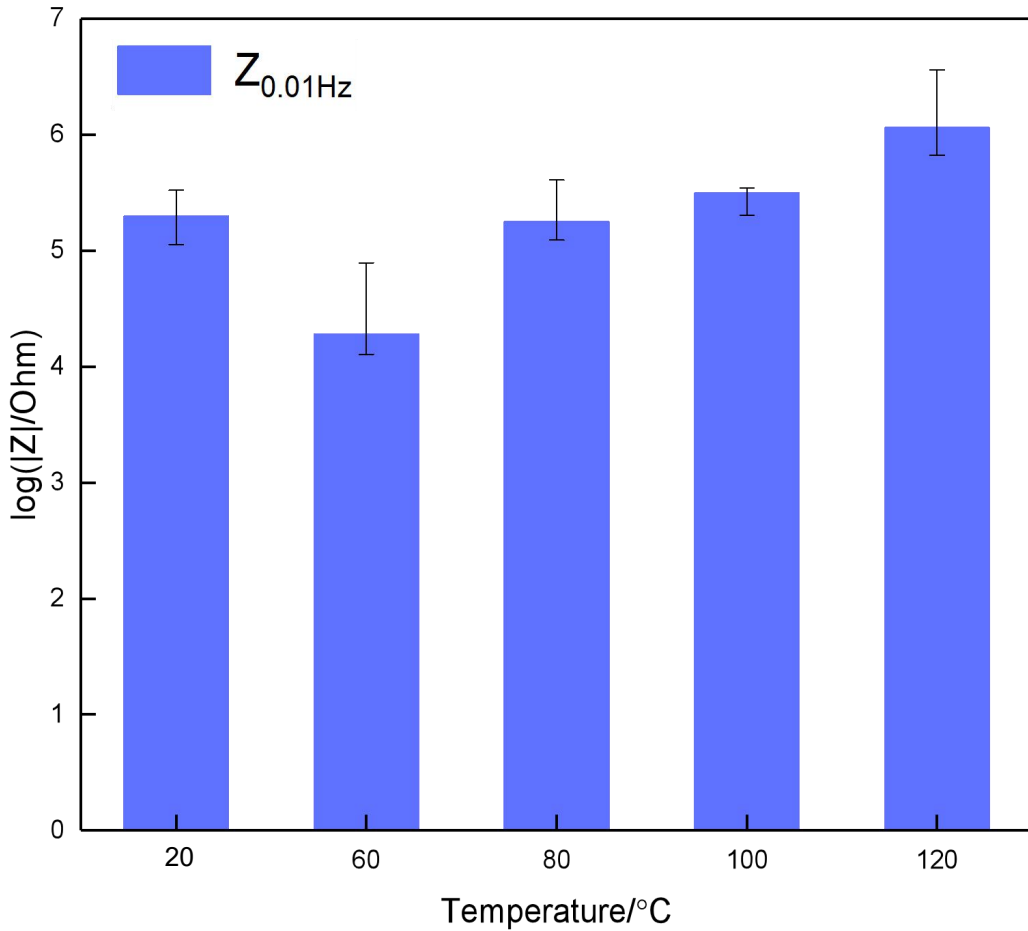
An active corrosion protection ability was examined by the immersion test and EIS of scribed AA2024-T3 coated with different sol-gel coatings. The immersion test was carried out in 0.5M NaCl solution for 7 days. The evolution of corrosion and active corrosion protection was monitored by digital optical microscope. Then, electrochemical properties of scribed coatings were evaluated with EIS measurements.

Immersion test

Figure 4.7 presents digital images of scribed GTS, GTS-Li-3%, GTS-Ce-3% and GTS-Li-Ce-1.5% coatings before and after different time of immersion in the 0.5 M NaCl solution.

The corrosion of scribed GTS coatings progressed with the immersion time. After 1 day of immersion, the scribe is filled with corrosion products. After 2 days immersion, the corrosion at the intersection of the scribe starts, the width of the scribe increased over 3 days immersion and some corrosion products inside the scribe were observed. After 7 days, the corrosion is spread all around the scribe, the scribe was full of the corrosion products and the surface of the sample was also damaged.

The corrosion process of scribed GTS-Li-3% was similar to that of GTS coatings. As shown in Figure 4.7 b), After 1 day the scribe is filled. After 7 days, the corrosion products spread all around which is the similar behavior as GTS coatings at the same time. The width of the scribe is increasing with immersion time. There are some white areas at the cross of the scribe, which could be associated with the corrosion protection by lithium leaching out from the coatings [46-48]. After 7 days immersion, the surface of the sample was corroded and the scribe was filled by the corrosion products. The amount of corrosion products was much less than that of the scribed GTS coatings, showing better corrosion protection of GTS-Li-3% compared to GTS coatings.

The corrosion progression of scribed GTS-Ce coatings was different from the GTS and GTS-LiNO$_3$-3% coatings. As shown in Figure 4.6 c). After 1 day of immersion, some white precipitation observed It was assumed to be CeO$_2$ [55,57]. Some corrosion products are also observed. After 7 days the surface is different, the scribe is not spreading and the white precipitated products are observed. these precipitates provided the active corrosion protection by forming CeO$_2$ [54,55]. These products protect the scribe against spreading.

The corrosion of scribed GTS-Li-Ce coatings was the slowest among all four samples. As

shown in Figure 4.6 d), After 1 day, some corrosion product (as shown with the red circle) was observed. After 2 days immersion, this circle disappeared with the help of self-healing of the coating. White precipitations could be CeO_2 and Al-Li LDH at the same time to inhibit the corrosion from anodic and cathodic reaction [46-48,54]. After 7 days the scribe is still not filled due to the synergistic effect of Ce and Li. The width of the scribe did not increase. In first 3 days immersion, the intact area of GTS-Li-Ce coatings were only corroded slightly. Few black dots are observed near the scribe. After 7 days immersion, some corrosion products were found far away from the cross of the scribe. The corrosion of the unscribed area was also slight. The scribes were not filled with corrosion products and the protection layer (white precipitates) can be observed

Overall, based on the immersion test, the best corrosion protection was provided by the GTS-Li-Ce coatings. The GTS-Ce coating had better protection compared to GTS-Li coating.
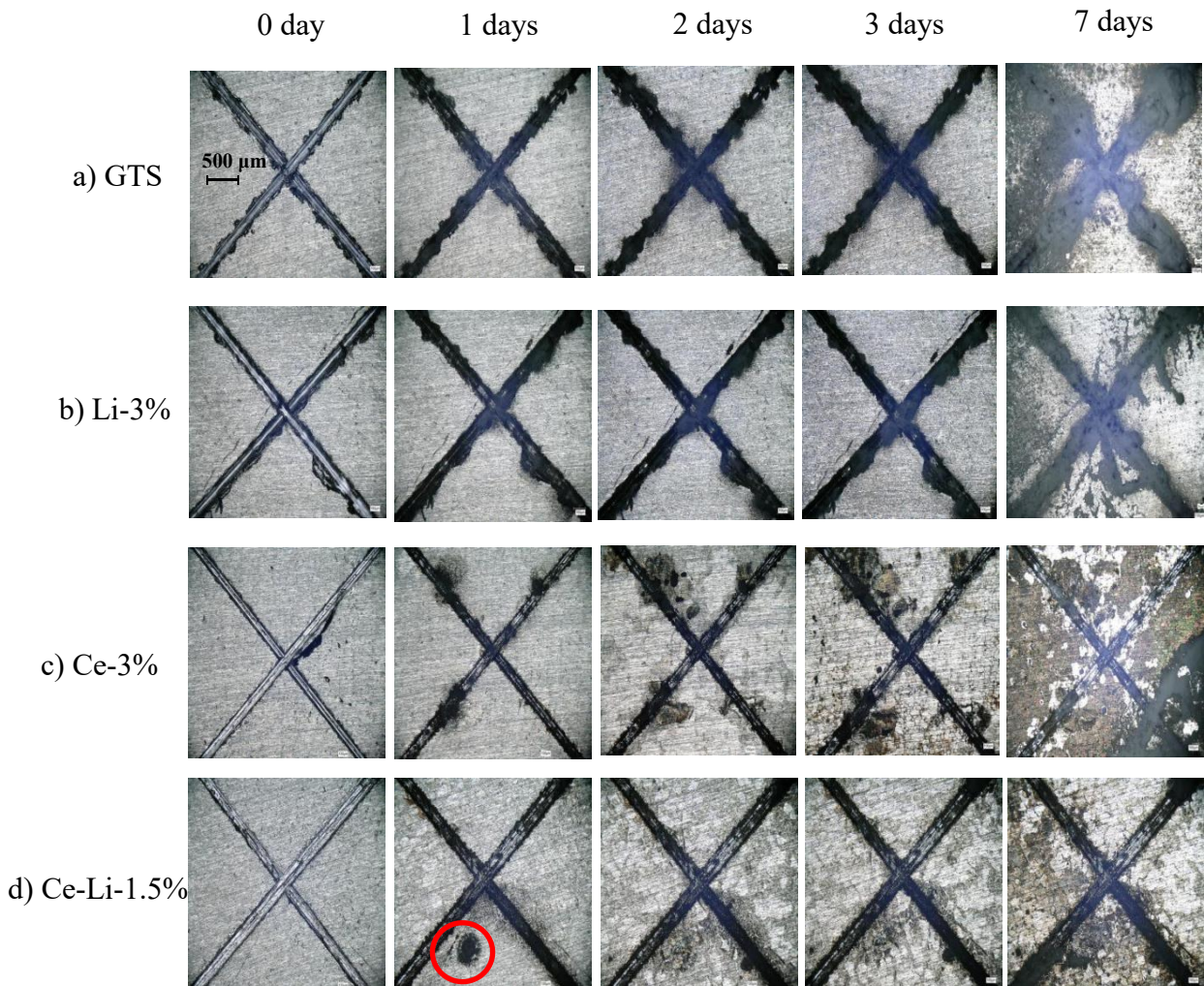

Figure 4.7. Optical microscope images of the scribed AA2024-T3 samples coated with a) GTS, b) GTS-LiNO3-3%, c) GTS-Ce, d) GTS-Li-Ce-1.5% with various immersion times in 0.5 M NaCl

Electrochemical impedance spectroscopy (EIS)

As shown in Figure 4.8, the value of impedance at 0.01 Hz in the Bode plot of impedance vs. frequency was extracted to plot against the various immersion time. The trend of corrosion resistance changing along the immersion time was represented by it. We made three repetitions and each of them is presented in separated plot (Fig.4.8 a, b, c). The Bode plots of all three repetitions are plotted separately in the appendix (Figure 6, 7 and 8).

The $Z_{0.01}$Hz value of scribed samples with GTS coatings decreased with immersion time over the 14 days in all three repetitions. After 2 days of immersion, the impedance decreased obviously. The value of impedance never returned. For the first 2 repetitions, the value of $Z_{0.01}$Hz were started around 3.9×10^4 Ohm/cm^2, while the value for the last repetition was relatively low, around 1.8×10^4 Ohm/cm^2.

The $Z_{0.01}$Hz value of scribed samples with GTS-Li-3% coatings were not in same trend in all three repetitions. In general, after 1 day of immersion, the modulus of impedance increased, then it decreased with immersion time until 7 days. In Figure 4.8 b), the impedance increased constantly until 7 days of immersion to reach the maximum value, while in 4.8 a) and c), the impedance reached its maximum value after 2 days of immersion. After 7 days immersion, there was a small increase (Fig 4.8 a and c). Then the impedance decreased until 14 days of immersion. The small increase may be related to the self-healing of GTS-Li-3% coatings. In three repetitions of GTS-Li-3% coatings, the returning of impedance modulus can be noticed, though the time of immersion were not the same.

The trend of $Z_{0.01}$Hz value of scribed samples with GTS-Ce-3% coatings were also different. After 1 day of immersion, the modulus of impedance increased (Figure 4.8 a, c), then it decreased in Figure 4.8 a) until the end of immersion, while in Figure 4.8 c), it stayed at relatively high value until 7 days of immersion and then decreased. After 7 days of immersion, the value of impedance dropped in Figure 4.8 b) and a small increase coming after. Also in all repetitions of GTS-Ce-3% coatings, the impedance increased after different time of immersion.

The trend of $Z_{0.01}$Hz value of scribed samples with GTS-Li-Ce-1.5% coatings were unique in all repetitions. After 1 day of immersion, the impedance increased and stayed at a stable value until 7 days of immersion (Fig 4.8 a, b). After 7 days immersion, the impedance of GTS-Li-Ce coatings reduced clearly until the end of measurements. In Figure 4.8 c), the impedance decreased to the minimum value until 3 days of immersion and then increased to the maximum impedance after 8 days of immersion. Then the formed protective layer may be destroyed since the impedance dropped fast after that.

To conclude, the self-healing effect of GTS-Li-3%, GTS-Ce-3% and GTS-Li-Ce-1.5%

coatings can be confirmed by the EIS results. Though due to the inhomogeneity of coating itself, there is no stable trend can be concluded. But with the addition of lithium and cerium as corrosion inhibitors, the returning of impedance values can be observed. With the help of immersion test, the active corrosion protection was confirmed in the case of GTS-Li-3%, GTS-Ce-3% and GTS-Li-Ce-1.5% coatings.
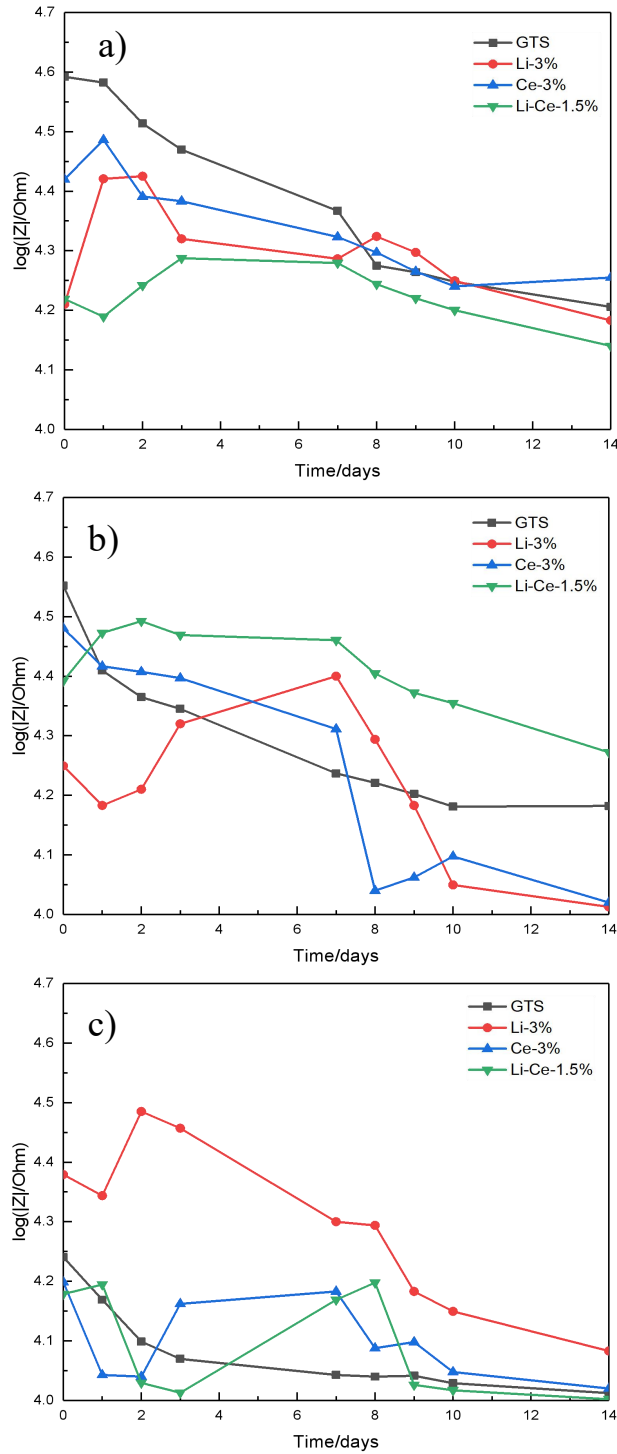

Figure 4.8. Three repetitions of values of $Z_{0.01Hz}$ (impedance at 0.01 Hz obtained from Bode plots in the appendix, Figure 6, 7 and 8) for different scribed coatings on AA2024-T3 as a function of time in 0.1 M NaCl solution

5 Conclusions

Corrosion protection of lithium salts and cerium salts on AA2024-T3 was studied in this thesis. Electrochemical methods including potentiodynamic polarization measurements and electrochemical impedance spectroscopy (EIS) were implemented to study the corrosion protection performance of different lithium salts, cerium salt and the synergic effect of both. The digital optical microscope was also used to investigate the active corrosion protections of the lithium and cerium inhibitors.

According to the results discussed above:

The GTS coatings could lower the corrosion current by an order of magnitude compared to that of the substrate AA2024-T3 and provide good barrier properties. Addition of the corrosion inhibitors could lower the corrosion current by an order of magnitude with respect to that of GTS coatings.

The combination of $LiNO_3$ and Ce $(NO_3)_3$ provides the best corrosion protection of intact coatings which is indicated by the lowest corrosion current and higher corrosion potential compared to the GTS-Ce-3% coatings.

The combination of $LiNO_3$ and Ce $(NO_3)_3$ also keeps the highest modulus of impedance at low frequency range in the first week. It indicates that the corrosion resistance of the GTS-Li-Ce-1.5% coating is the best among all the intact coatings.

From 60 to 120°C, higher curing temperatures ensure the higher value of impedance of the GTS coatings, which means the better corrosion protection of GTS coating applied on the AA20244-T3. The samples cured at room temperatures also show relatively good corrosion resistance, but the details need to be investigated further.

The addition of inhibitors could also provide good active corrosion protection for the scribed AA2024-T3 with GTS coatings. The modulus of the impedance of the coatings with inhibitors at 0.01 Hz all increase with the corrosion progression. The morphologies of GTS-Li-Ce-1.5% coating of different immersion time show the best corrosion protection for scribed coatings compared to others.

Base on the results above, further researches and experiments need to be carried out from the following fields: (1) the effect of LiOH as a corrosion inhibitor needs further investigation, and whether LiOH can work with $Ce(NO_3)_3$ to provide corrosion protection is unknown. (2) The mechanism of synergistic effect of lithium salts and cerium salts is not clear. The experimental evidence is needed. (3) The effect of the curing temperature needs more experiments to verify the conclusion. (4) The effects of lithium inhibitor, lithium inhibitor incorporating with cerium inhibitor on the corrosion protection for different aluminium alloys e.g. AA7075-T6 need to be studied.

6   Acknowledgement

I would like to express my sincere gratitude to all the people who have provided so much help for me during my graduation project.

Firstly, I am so much grateful to my supervisor Prof. Arjan Mol who gave me this precious opportunity to study and do research on the topic of corrosion. At the same time, your guidance and support on my thesis are also very important to me.

Secondly, I would like to thank my daily supervisor Dr. Urša Tiringer, who walked me through my thesis step by step and spent countless amount of time to help me on both practical and theoretical aspects. without your help, I cannot make it.

Then, my thanks would also go to the members of corrosion group who inspired me during the experiments and gave me many useful tips to assure the success of my experiments. I would also like to thank the lab technician Agnieszka Kooijman-Banaszak who solved lots of problems I have met during the whole experiments. I would also like to give my gratitude to Dr. Peter Visser from AkzoNobel for provide many creative thoughts and methods of experiments to help me conduct the experiments successfully.

Last, I would like to thank my family for their support and encouragement in my life. Thank them for supporting my decision of studying abroad and giving me this opportunity to experience a totally different life. They are the source of my power to reach my goals.

Two-year master program in TU Delft is a very valuable experiment for me to grow my academic ability. As the most important part of the master program, this graduation thesis has provided me solid fundamentals both practically and theoretically for my further PhD study. I think what I have learned during these two years would benefit me through my whole life. Thank you all again!!

References

[1]   WorldAtlas, The most abundant elements in the earth's crust, (2018). https://www.worldatlas.com/articles/the-most-abundant-elements-in-the-earth-s-crust.html.

[2]   Aalco, Aluminium Alloy: Introduction to Aluminium and its alloys, http://www.aalco.co.uk/datasheets/Aluminium-Alloy_Introduction-to-Aluminium-and-its-alloys_9.ashx.

[3]   J. G. Kaufman, *Introduction to aluminum alloys and tempers*, ASM International, 2000.

[4]   R. B. Figueira, C. J. R. Silva, E. V. Pereira, Organic–inorganic hybrid sol–gel coatings for metal corrosion protection: a review of recent progress, *J. Coat. Technol. Res*, 12(1) 1-35,2015.

[5]   S. Benavides, *Corrosion Control in the Aerospace Industry*, Woodhead Publ Ltd, Cambridge, 2009.

[6]   Vargel C. *Corrosion of aluminium*. 1st ed. Amsterdam, The Netherlands: ELSEVIER; 2004.

[7]   Davis J. R. Corrosion of aluminum and aluminum alloys. 1st ed. United States of America: ASM International; 1999: 10-23.

[8]   Kufman G. *Introduction to aluminum alloys and tempers*. 1st ed. ASM International; 2000.

[9]   N. Birbilis and R. G. Buchheit, "Investigation and Discussion of Characteristics for Intermetallic Phases Common to Aluminum Alloys as a Function of Solution pH," *J. Electrochem. Soc.*, vol. 155, no. 3, pp. C117–C126, Jan. 2008.

[10]   A. E. Hughes, B. Hinton, S. A. Furman, I. S. Cole, D. Paterson, A. Stonham, G. McAdam, D. Dixon, S. J. Harris, A. Trueman, M. Hebbron, C. Bowden, P. Morgan and M. Ranson, Corrosion Reviews 25 (2007) 275.

[11]   Fundamentals of Flight, Shevell, Richard S, 1989, Englewood Cliffs, Prentice Hall, ISBN 0-13-339060-8, Ch 18, pp 373-386.

[12]   The-Aluminum-Association, International Alloy Designations and Chemical Composition Limits for Wrought Aluminum and Wrought Aluminum Alloys, 2015.

[13]   Metals Handbook, Vol.2 - Properties and Selection: Nonferrous Alloys and Special-Purpose Materials, ASM International 10th Ed. 1990.

[14]   A.Boag, A.E. Hughes, N.C. Wilson, How complex is the microstructure of AA2024-T3?, corrosion science 51 (2009) 1565-1568.

[15]   R. G. Buchheit, M. A. Martinez, and L. P. Montes, "Evidence for Cu Ion Formation by Dissolution and Dealloying the Al2CuMg Intermetallic Compound in Rotating Ring-Disk Collection Experiments," J. Electrochem. Soc., vol. 147, no. 1, pp. 119–124, Jan. 2000..

[16]   E. Bardal, *Corrosion and Protection*, 1st ed., Springer-Verlag, London, 2004.

[17]   E. McCafferty, Introduction to Corrosion Science, 1st ed., Springer Science+Business Media, New York, 2010.

[18]   M. Cerit, Corrosion pit-induced stress concentration in spherical pressure vessel, Thin-Walled Struct. 136 (2019) 106–112. doi:10.1016/j.tws.2018.12.014.

[19]   Pourbaix, M., Atlas of electrochemical equilibria in aqueous solutions. 2d English ed. 1974, Houston, Tex.: National Association of Corrosion Engineers.

[20]   N.L. Sukiman, X. Zhou, N. Birbilis, J.M.C. Mol, S.J. Garcia, G.E. Thompson, Durability and Corrosion of Aluminium and Its Alloys: Overview, Property Space, Techniques and Developments, in: Z. Ahmad (Ed.), Alum. Alloy. - New Trends Fabr. Appl., IntechOpen, London, 2013: pp. 47–98.

[21]   Norio Sato. An overview on the passivity of metals. Corrosion science, 31:1–19, 1990.

[22]   Marcel Pourbaix. Atlas of electrochemical equilibria in aqueous solution. NACE, 307,1974.

[23]   M. G. Fontana and N. D. Greene, in "Corrosion Engineering" (McGraw-Hill, London, 1967) p. 28.

[24]   Bogar F.D., Foley F.D., The influence of chloride ion on the pitting of aluminium, Journal of the Electrochemical Society, vol. 119, 1973, p. 462–464.

[25]   Godard H.P., The corrosion behavior of aluminium in natural waters, The Canadian Journal of Chemical Engineering, vol. 38, 1960, p. 167–173.

[26]   J. Evertsson, F. Bertram, F. Zhang, L. Rullik, L.R. Merte, M. Shipilin, M. Soldemo, S. Ahmadi, N. Vinogradov, F. Carlà, J. Weissenrieder, M. Göthelid, J. Pan, A. Mikkelsen, J.O. Nilsson, E. Lundgren, The thickness of native oxides on aluminum alloys and single crystals, Appl. Surf. Sci. 349 (2015) 826–832. doi:10.1016/j.apsusc.2015.05.043.

[27]   Chongchong chen. Formation and stability of lithium protective layer for corrosion protection of AA2024-T3 and AA2198-T8 aluminum alloys, Master diss, Delft University of technology, 2020.

[28]   Feldman, D. Polymer Barrier Films. Journal of Polymers and the Environment 9, 49–55 (2001).

[29]   Sviatlana V. Lamaka Snihirova, Darya and M. Fatima Montemor. Smart composite coatings for corrosion protection of aluminium alloys in aerospace applications. Smart Composite Coatings and Membranes, pages 85–121, 2016.

[30]   Ursa Tiringer, Janez Kovac, Ingrid Milosev. Effects of mechanical and chemical pre-treatments on the morphology and composition of surfaces of aluminium alloys 7075-T6 and 2024-T3. Corrosion science, 119(1): 46-59, 2017.

[31]   M. W. Kendig and R. G. Buchheit, "Corrosion Inhibition of Aluminum and Aluminum Alloys by Soluble Chromates, Chromate Coatings, and Chromate-Free Coatings," CORROSION, vol. 59, no. 5, pp. 379–400, May 2003.

[32]   Directive 2002/95/EC of the European Parliament and of the Council of 27 January 2003 on the restriction of the use of certain hazardous substances in electrical and electronic equipment, vol. OJ L. 2003.

[33]   J. W. Bibber, "An overview of non-hexavalent chromium conversion coatings— Part I: aluminum and its alloys," Metal Finishing, vol. 99, no. 12, pp. 15–22, Dec. 2001.

[34]   H. Wang and R. Akid, "Encapsulated cerium nitrate inhibitors to provide high-performance anti-corrosion sol–gel coatings on mild steel," Corrosion Science, vol. 50, no. 4, pp. 1142–1148, Apr. 2008

[35]   C. J. Brinker, A. J. Hurd, P. R. Schunk, G. C. Frye, and C. S. Ashley, "Review of sol-gel thin film formation," Journal of Non-Crystalline Solids, vol. 147, pp. 424–436, Jan. 1992.

[36]   Rita B. Figueira, Isabel R. Fontinha, Carlos J. R. Silva, and Elsa V. Pereira, "Hybrid Sol-Gel Coatings: Smart and Green Materials for Corrosion Mitigation," Coatings, vol. 6, no. 1, p. 12, Mar. 2016.

[37]   S. Zheng and J. Li, "Inorganic–organic sol gel hybrid coatings for corrosion protection of metals," J Sol-Gel Sci Technol, vol. 54, no. 2, pp. 174–187, May 2010

[38]   M. L. Zheludkevich, I. M. Salvado, and M. G. S. Ferreira, "Sol–gel coatings for corrosion protection of metals," J. Mater. Chem., vol. 15, no. 48, pp. 5099–5111, Dec. 2005.

[39]   C. J. Brinker, A. J. Hurd, P. R. Schunk, G. C. Frye, and C. S. Ashley, "Review of sol-gel thin film formation," Journal of Non-Crystalline Solids, vol. 147, pp. 424–436, Jan. 1992.

[40]   A ´ lvarez, D, Collazo, A, Herna´ndez, M, No´ voa, XR, Pe´ rez,C,

''Characterization of Hybrid Sol–Gel Coatings Doped with Hydrotalcite-Like Compounds to Improve Corrosion Resistance of AA2024-T3 Alloys.'' Prog. Org. Coat., 67 152–160 (2010).

[41]   D. Álvarez, A. Collazo, M. Hernández, X. R. Nóvoa, and C. Pérez, "Characterization of hybrid sol–gel coatings doped with hydrotalcite-like compounds to improve corrosion resistance of AA2024-T3 alloys," Progress in Organic Coatings, vol. 67, no. 2, pp. 152–160, Feb. 2010.

[42]   Dariva, G., Gallo, A. (2014). Corrosion Inhibitors – Principles, Mechanisms and Applications. Developments in Corrosion Protection. Intech Open.

[43]   Andreatta, F., & Fedrizzi, L. (2016). Corrosion Inhibitors. In Active Protective Coatings (pp. 59–83). Springer.

[44]   Gerald S. Frankel and Richard L. Inhibition of al alloy corrosion by chromates. Interface-Electrochemical Society, 10(4):34–39, 2001.

[45]   M. W. Kendig and R. G. Buchheit. Corrosion inhibition of aluminum and aluminum alloys by soluble chromates, chromate coatings, and chromate-free coatings. Corrosion, 59(5):379–400, 2003.

[46]   Peter Visser, Mats Meeusen, Yaiza Gonzalez-Garcia, Herman Terryn, and Johannes M. C. Mol. Electrochemical Evaluation of Corrosion Inhibiting Layers Formed in a Defect from Lithium-Leaching Organic Coatings, Journal of The Electrochemical Society, 164 (7) C396-C406 (2017).

[47]   Peter Visser. The corrosion protection of AA2024-T3 aluminium alloy by leaching of lithium-containing salts from organic coatings. Faraday discussions, 180:511–526, 2015.

[48]   Peter Visser, Yaiza Gonzalez-Garcia, Johannes M. C. Mol, and Herman Terryn, Mechanism of Passive Layer Formation on AA2024-T3 from Alkaline Lithium Carbonate Solutions in the Presence of Sodium Chloride, Journal of The Electrochemical Society, 165 (2) C60-C70 (2018).

[49]   P. A. Schweitzer, Corrosion and Corrosion Protection Handbook, M. Dekker (1989).

[50]   G. R. Williams and D. O'Hare, J Phys Chem B, 110, 10619 (2006).

[51]   B.R.W.Hinton, Corrosion inhibition with rare earth metal salts, Journal of Alloys an Compounds, 180(1992): 15-25.

[52]   A. J. Aldykiewicz, A. J. Davenport, and H. S. Isaacs, J. Electrochem. Soc., 143, 147(1996).

[53]   K. A. Yasakau, M. L. Zheludkevich, S. V. Lamaka, and M. G. S. Ferreira, J. Phys.Chem. B, 110, 5515 (2006).

[54]   Urša Tiringer, Ingrid Milošev, Alicia Durán, Yolanda Castro. Hybrid sol–gel coatings based on GPTMS/TEOS containing colloidal SiO_2 and cerium nitrate for increasing corrosion protection of aluminium alloy 7075-T6, Journal of Sol-Gel Science and Technology (2018) 85:546–557.

[55]   Ursa Tiringer, Alicia Dur´an, Yolanda Castro, and Ingrid Milosev. Self-Healing Effect of Hybrid Sol-Gel Coatings Based on GPTMS, TEOS, SiO2 Nanoparticles and Ce(NO3)3 Applied on Aluminum Alloy 7075-T6. Journal of The Electrochemical Society, 165 (5) C213-C225 (2018).

[56]   R. G. Buchheit, M. A. Martinez, and L. P. Montes, J. Electrochem. Soc., 147, 119 (2000).

[57]   B. Poulson, Electrochemical measurements in flowing solutions, Corros. Sci. 23 (1983) 391–430.

[58]   Branko N. Popov. Chapter 5 - Basics of Corrosion Measurements, Corrosion Engineering, pages 181–237. Elsevier, 2015.

[59]   J. Tafel, Polarization during cathodic hydrogen development, Z. Phys. Chem. 50 (1904) 641–712.

[60]   Allen J Bard, Larry R Faulkner, Johna Leddy, and Cynthia G Zoski. Electrochemical methods: fundamentals and applications, volume 2. wiley New York, 1980

[61]   D Needham. Reverse engineering of the low temperature-sensitive liposome (ltsl) for treating cancer. In Biomaterials for Cancer Therapeutics, pages 270–353e. Elsevier, 2013.

[62]   Milton Stern and Al L Geary. Electrochemical polarization i. a theoretical analysis of the shape of polarization curves. Journal of the electrochemical society, 104(1):56–63, 1957.

[63]   Florian Mansfeld. Recording and analysis of ac impedance data for corrosion studies. Corrosion, 37(5):301–307, 1981.

[64]   I. Epelboin. The dissolution and passivation of fe and fecr alloys in acidified sulphate medium: Influences of ph and cr content. Corrosion Science, 19(5):1105–1112, 1979.

[65]   Optieis: A multisine implementation application note rev. 1.0. 1990-2011.

[66]   David Loveday, Pete Peterson, and Bob Rodgers. Evaluation of Organic Coatings

with Electrochemical Impedance Spectroscopy, Part 1: Fundamentals of Electrochemical Impedance Spectroscopy. JCT Coatings Tech, 46-52, 2004.

[67]   Vadim F Lvovich. Impedance spectroscopy: applications to electrochemical and dielectric phenomena,page 4. John Wiley & Sons, 2012.

[68]   Application Note AC- 1, Subject: Basics of Electrochemical Impedance Spectroscopy. Princeton Applied Research.

[69]   Yanwen Liu, Peter Visser, Xiaorong Zhou, Stuart B. Lyon, Teruo Hashimoto, Michele Curioni, Ali Gholinia,a George E. Thompson, Gerard Smyth, Simon R. Gibbon, Derek Graham, Johannes M. C. Mol, and Herman Terryn. Protective Film Formation on AA2024-T3 Aluminum Alloy by Leaching of Lithium Carbonate from an Organic Coating. Journal of The Electrochemical Society, 163 (3) C45-C53 (2016).

Appendix
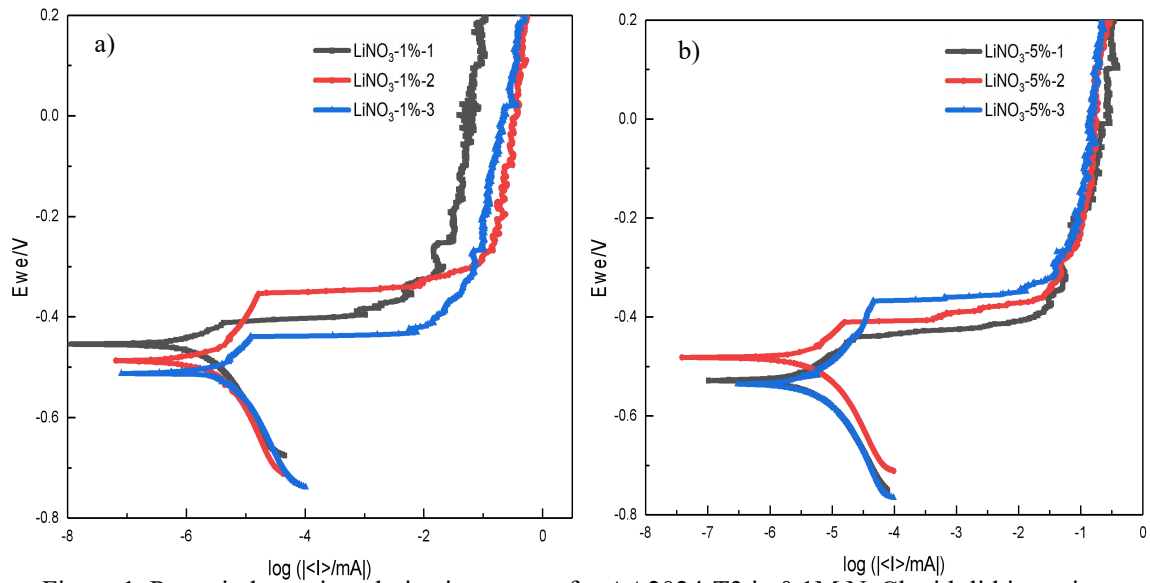
Figure 1. Potentiodynamic polarization curves for AA2024-T3 in 0.1M NaCl with lithium nitrates as corrosion inhibitor, a) GTS-LiNO3-1%, b) GTS-LiNO3-5%
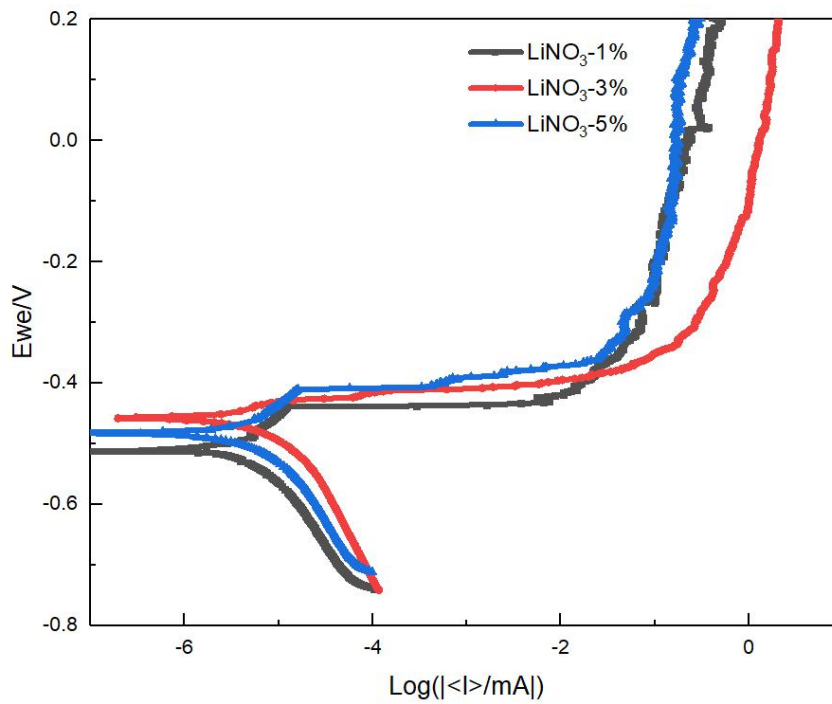

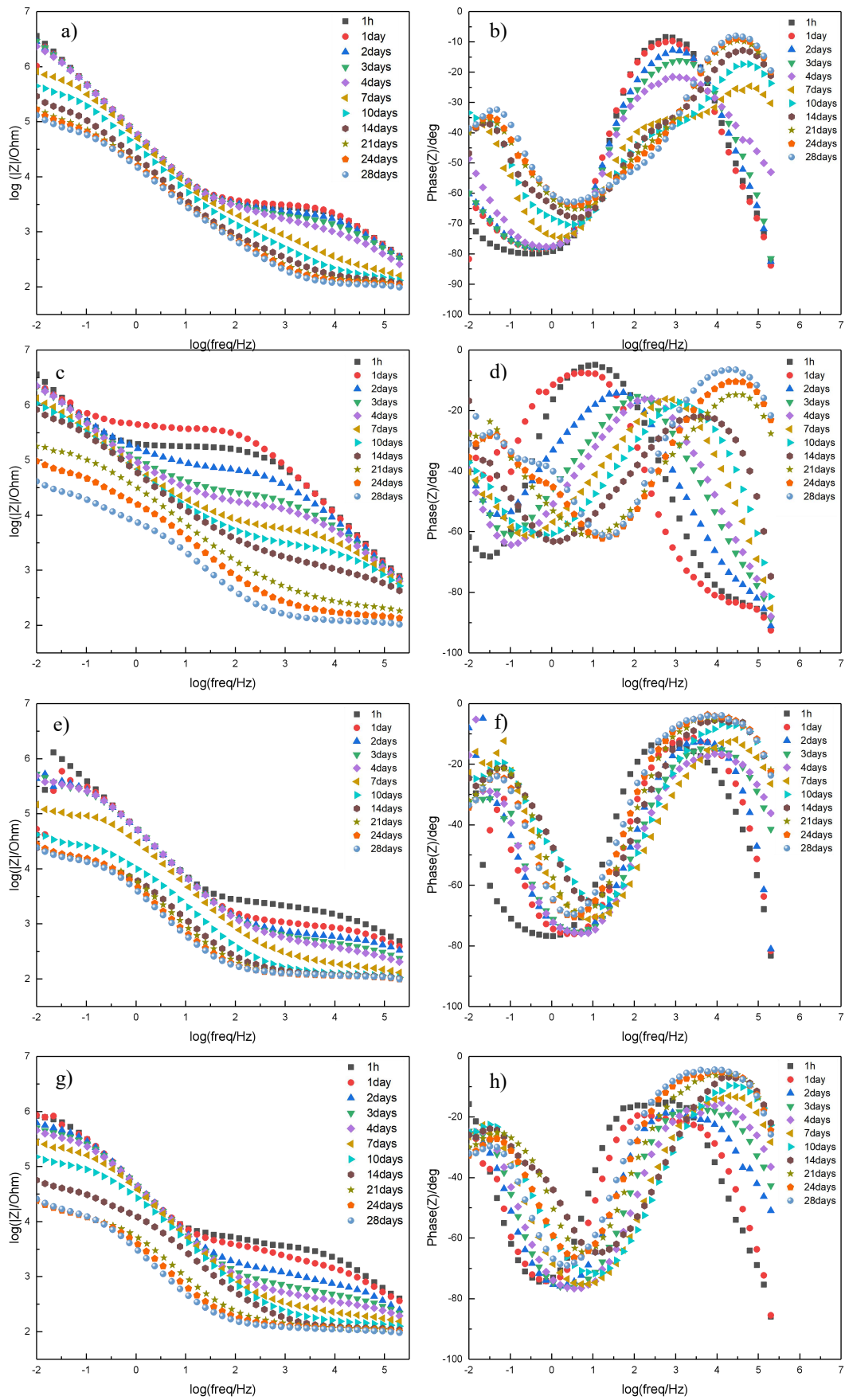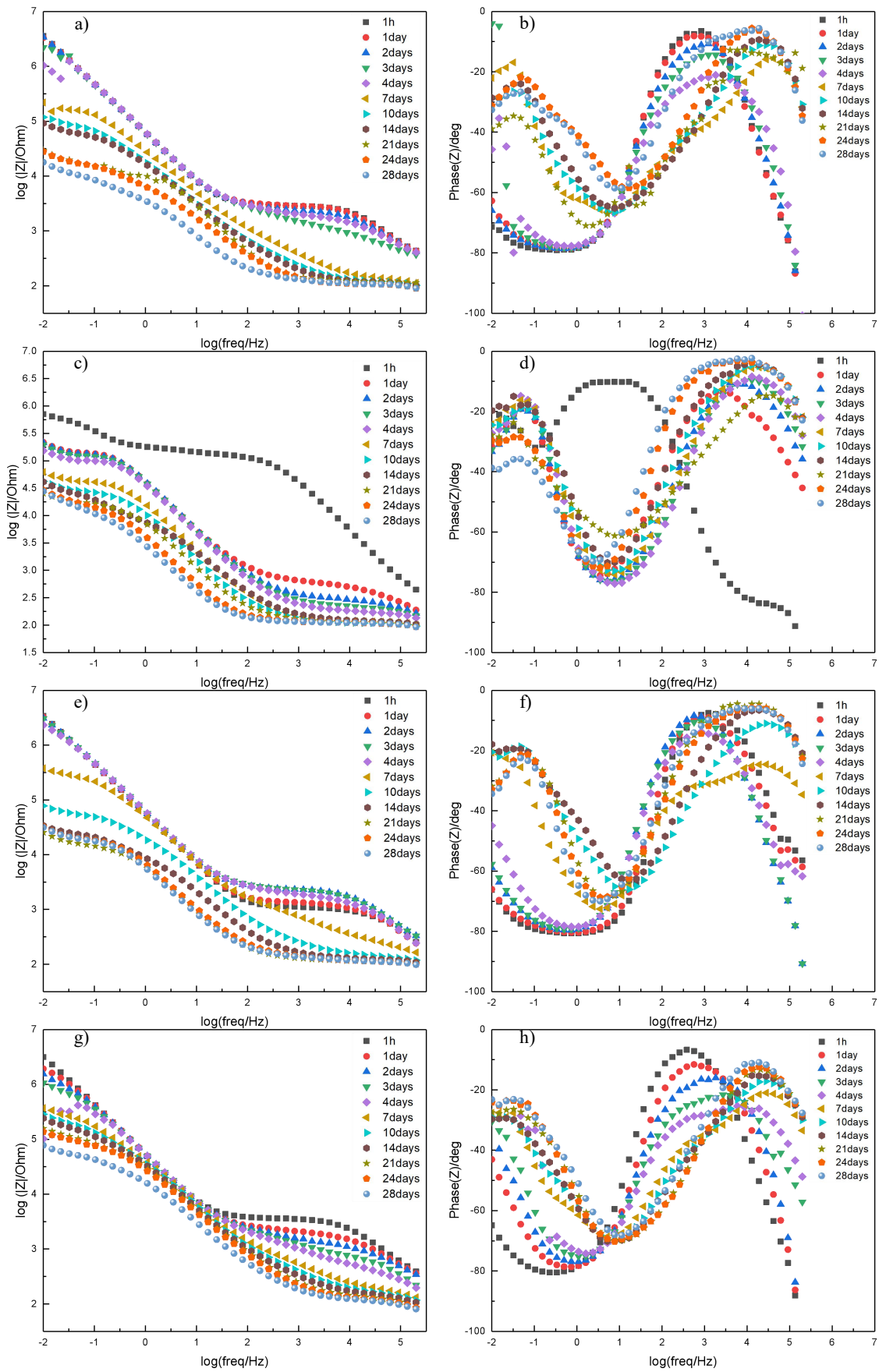Figure 2. The comparison of polarization curves with lithium nitrates of different concentrations

Figure 3. Bode plots of impedance and phase angle vs. frequency for AA2024-T3 in 0.1M NaCl with and without corrosion inhibitor for 28 days, (a, b) GTS, (c, d) GTS-Ce-3%(e, f) GTS-Li-3%, (g, h) GTS-Li-Ce-1.5%-- (2)
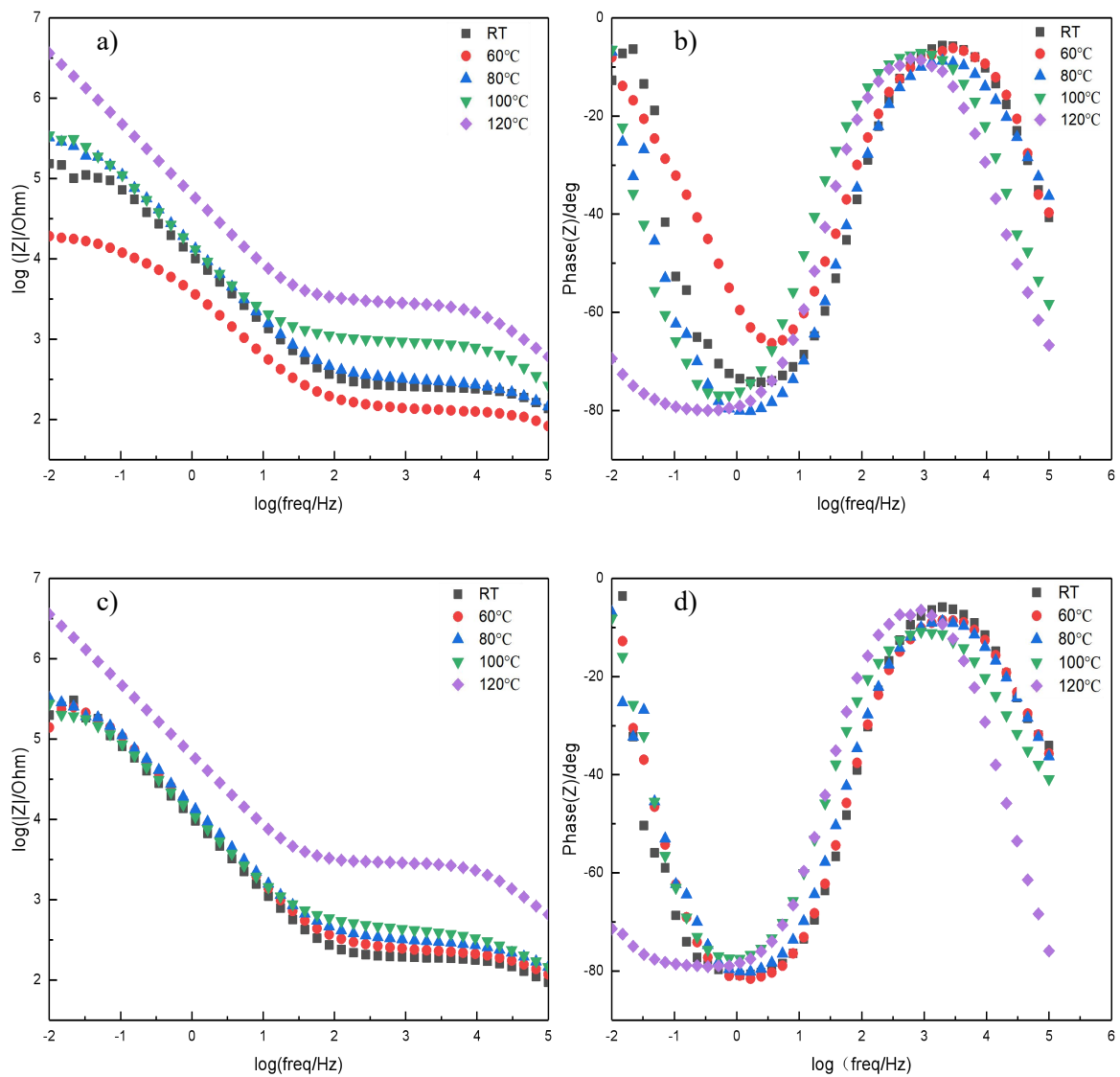
Figure 4. Bode plots of impedance and phase angle vs. frequency for AA2024-T3 in 0.1M NaCl with and without corrosion inhibitor for 28 days, (a, b) GTS, (c, d) GTS-Ce-3%(e, f) GTS-Li-3%, (g, h) GTS-Li-Ce-1.5% --(3)

Figure 5. Bode plots of impedance and phase angle vs. frequency for AA2024-T3 in 0.1M NaCl without corrosion inhibitor of different curing temperatures (second and third repetitions)
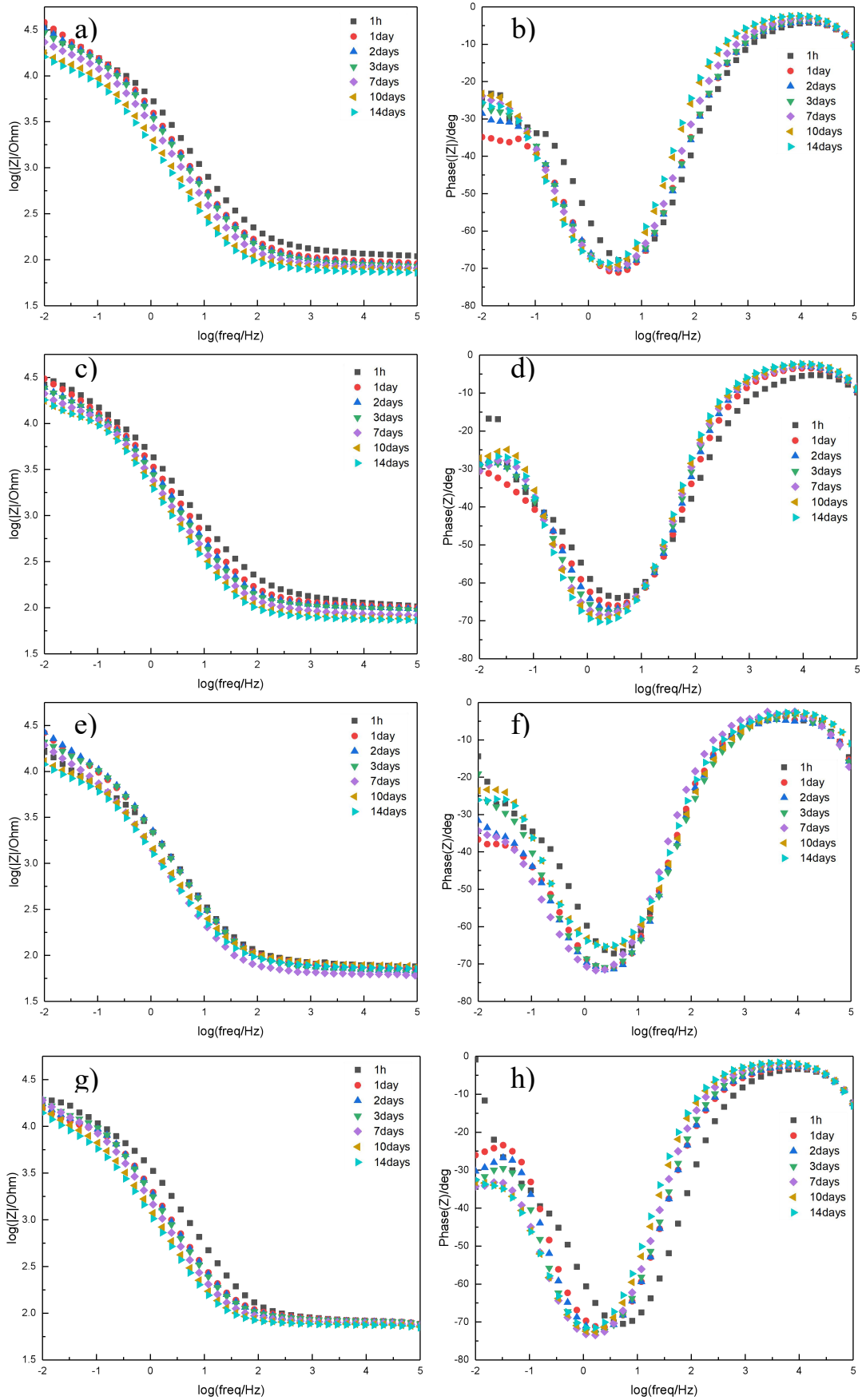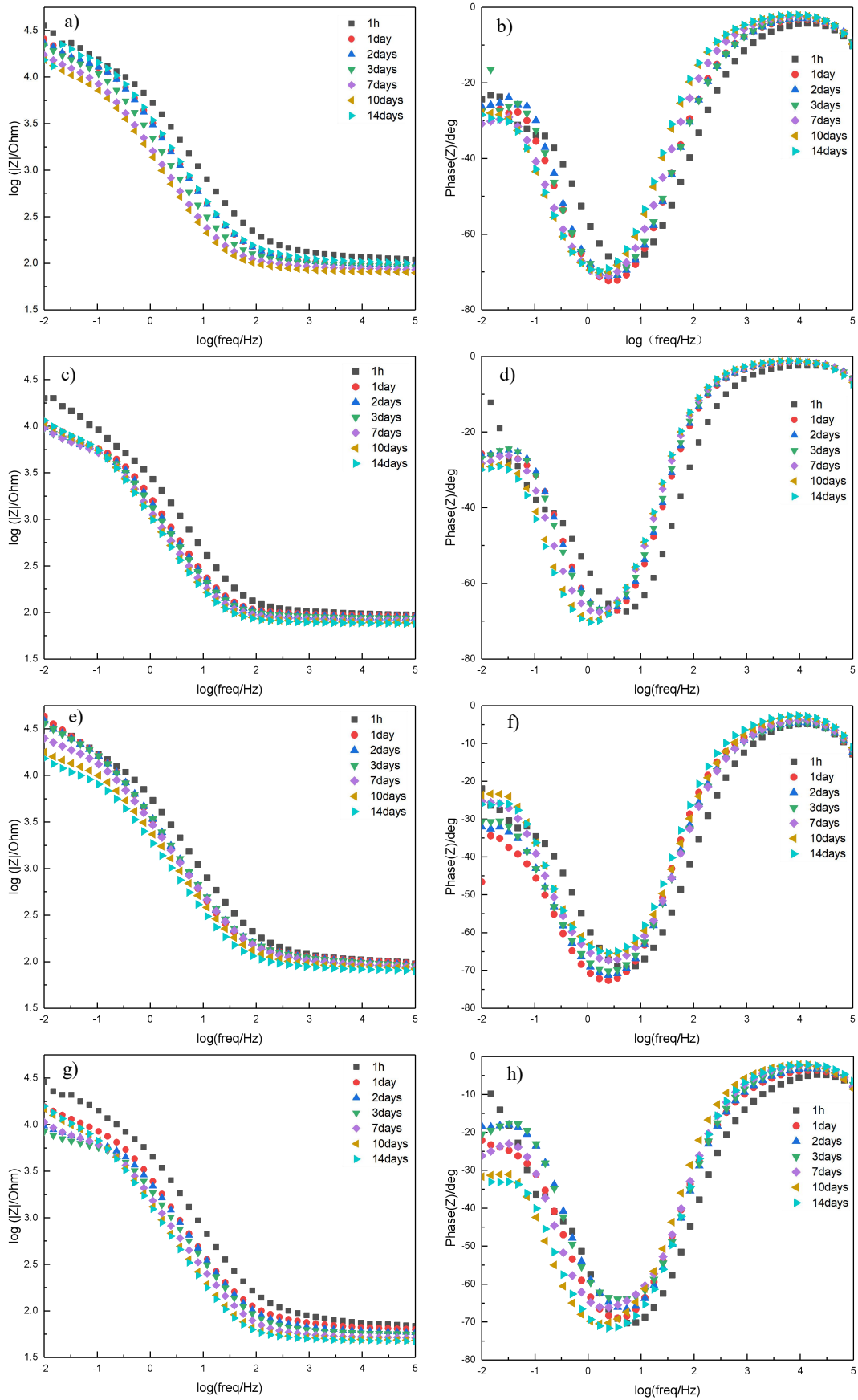
Figure 6. Bode plots of impedance and phase angle vs. frequency for scribed AA2024-T3 samples in 0.1M NaCl with and without corrosion inhibitor for 14 days, (a, b) GTS, (c, d) GTS-Ce (e, f) GTS-LiNO$_3$-3%, (g, h) GTS-Li-Ce-1.5% --(1)

Figure 7. Bode plots of impedance and phase angle vs. frequency for scribed AA2024-T3 samples in 0.1M NaCl with and without corrosion inhibitor for 14 days, (a, b) GTS, (c, d) GTS-Ce (e, f) GTS-LiNO$_3$-3%, (g, h)GTS-Li-Ce-1.5%--(2)
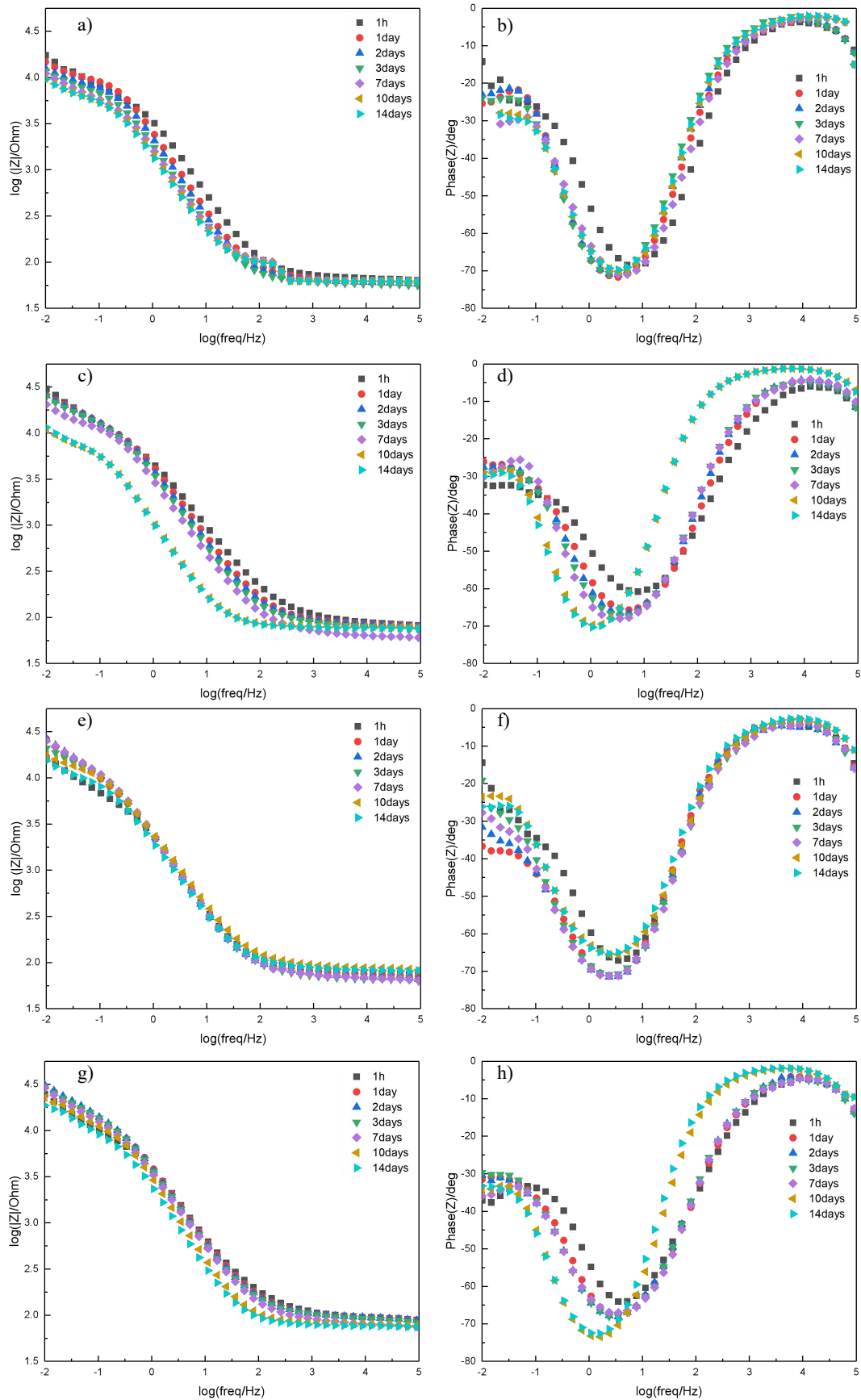
Figure 8. Bode plots of impedance and phase angle vs. frequency for scribed AA2024-T3 samples in 0.1M NaCl with and without corrosion inhibitor for 14 days, (a, b) GTS, (c, d) GTS-Ce (e, f) GTS-LiNO$_3$-3%, (g, h) GTS-Li-Ce-1.5%--(3)